Available online at www.sciencedirect.com

ScienceDirect

Geochimica et Cosmochimica Acta 238 (2018) 357–373

Geochimica et Cosmochimica Acta

www.elsevier.com/locate/gca

Magnesium isotopic composition of altered oceanic crust and the global Mg cycle

Kang-Jun Huang [a,b,*], Fang-Zhen Teng [b,*], Terry Plank [c], Hubert Staudigel [d], Yan Hu [b], Zheng-Yu Bao [e]

[a] State Key Laboratory of Continental Dynamics and Shaanxi Key Laboratory of Early Life and Environment, Department of Geology, Northwest University, Xi'an 710069, China

[b] Isotope Laboratory, Department of Earth and Space Sciences, University of Washington, Seattle, WA 98195, USA

[c] Lamont Doherty Earth Observatory, Columbia University, Palisades, NY 10964-8000, USA

[d] Institute of Geophysics and Planetary Physics, Scripps Institution of Oceanography, University of California, San Diego, La Jolla, CA 92093, USA

[e] State Key Laboratory of Geological Processes and Mineral Resources & Faculty of Earth Sciences, China University of Geosciences, Wuhan 430074, China

Received 6 October 2017; accepted in revised form 3 July 2018; Available online 11 July 2018

Abstract

To investigate the behavior of Mg isotopes during low-temperature alteration of oceanic crust and to further understand its role in the global Mg cycle, we measured the Mg isotopic compositions ($^{25}Mg/^{24}Mg$ and $^{26}Mg/^{24}Mg$) of a set of samples of altered oceanic crust (AOC) recovered from the Ocean Drilling Program Hole 801C, the reference site for old crust (~170 Ma) subducting in the Pacific. The measured $\delta^{26}Mg$ values range from −1.70‰ to 0.21‰, deviating from that of pristine oceanic basalts (−0.25 ± 0.07‰). Composite samples of volcanoclastic breccia that have experienced relatively intense alteration have larger variation in $\delta^{26}Mg$ values (−1.01‰ to 0.15‰) than composite samples of massive basaltic flows (−0.53‰ to −0.04‰), indicating significant Mg isotope fractionation during low-temperature alteration of the oceanic crust. Moreover, the upper off-axis basement has on average lower $\delta^{26}Mg$ values (−1.70‰ to −0.04‰) than the lower on-axis basement (−0.16‰ to 0.21‰). These findings, combined with the co-variations between MgO content and FeO^*/CaO ratio and between $\delta^{26}Mg$ and FeO^*/CaO ratio, suggest that formation of Mg-bearing minerals (i.e., saponite and calcite) during low-temperature alteration of the oceanic crust accounts for the highly variable $\delta^{26}Mg$ of AOC. Early formation of saponite under anoxic condition preferentially takes up heavy Mg isotopes and accounts for Mg enrichment and relatively high $\delta^{26}Mg$ in the on-axis basement. Subsequent precipitation of carbonates results in the dilution of Mg and relatively low $\delta^{26}Mg$ in the off-axis basement. In addition, accumulation of carbonate-rich interflow sediments in the upper basement may contribute further to the low $\delta^{26}Mg$. A weighted average $\delta^{26}Mg$ value of 0.00 ± 0.09‰ is estimated for the AOC at Site 801, implying that low-temperature alteration of oceanic crust drives the ocean to a lighter Mg isotopic composition, and thus requires additional carbonate precipitation to maintain a steady-state Mg isotopic composition of seawater. A mass balance calculation suggests that the Mg output flux due to low-temperature alteration of the oceanic crust equals ~12% of the annual Mg riverine input, indicating that AOC is a significant sink of Mg in seawater. Our study further highlights that recycling of AOC with highly variable

* Corresponding authors at: State Key Laboratory of Continental Dynamics and Shaanxi Key Laboratory of Early Life and Environment, Department of Geology, Northwest University, Xi'an 710069, China (K.-J. Huang).

E-mail addresses: hkj@nwu.edu.cn (K.-J. Huang), fteng@u.washington.edu (F.-Z. Teng).

https://doi.org/10.1016/j.gca.2018.07.011

δ^{26}Mg along with overlying marine sediments into the mantle through subduction may generate Mg isotopic heterogeneity in the mantle at small scales.

Keywords: Magnesium isotopes; Oceanic crust; Low-temperature alteration; Mg cycle; Mantle heterogeneity

1. INTRODUCTION

Oceanic crust undergoes extensive seawater alteration prior to subduction into trenches. This process not only modifies compositions of seawater and the upper oceanic crust (Hart et al., 1974; Seyfried et al., 1984; Elderfield et al., 1999; Chan et al., 2002), but also regulates long-term climate change by uptake of carbon (Staudigel et al., 1989, 1996; Alt and Teagle, 1999; Coogan and Gillis, 2013). Ultimately, the altered oceanic crust (AOC) is recycled into the mantle by subduction, making an important contribution to mantle heterogeneity (Hofmann, 1997; Kelley et al., 2005; Chauvel et al., 2008). Thus, knowledge of the composition of AOC is pivotal to understanding the cycling of elements and its impact on the composition of the Earth's mantle.

As a major element in both the silicate Earth and hydrosphere, Mg is critical in deciphering the chemical evolution of the oceans and change of the global climate, which is borne out by the co-variation between seawater Mg/Ca and climate throughout Earth's history (Hardie, 1996; Stanley and Hardie, 1998; Demicco et al., 2005). In general, Mg is transferred from continents to the oceans via river and groundwater discharge, and is sequestered mainly by carbonate deposition and alteration of the oceanic crust on the ridge axis and the ridge flank (Drever, 1974; Elderfield and Schultz, 1996). Based on heat flow anomalies and compositions of hot springs, between 10% and 40% of the riverine input of Mg is estimated to be taken up by hydrothermal alteration of the oceanic crust along the axis (Mottl and Wheat, 1994). A higher uptake flux of Mg is expected during low-temperature alteration of the oceanic crust on the ridge flank since approximately two-thirds of the hydrothermal heat is lost there (Mottl, 2003). However, accurate assessment of the Mg uptake flux associated with low-temperature alteration of the oceanic crust is still not clear due to the large variation in alteration temperature and the small change in composition of the ridge flank fluids (Staudigel, 2014). This hinders our understanding of the controlling factors on the cycling of Mg in the oceans and the linkage between climate and seawater chemistry.

Magnesium isotopes may provide a potential constraint on the geochemical cycling of Mg in the oceans and the magnitude of Mg flux into the oceanic crust during low-temperature alteration, because the main inputs and sinks of seawater Mg have distinctive isotopic compositions. The current riverine input has an average δ^{26}Mg value of −1.09‰ (Tipper et al., 2006), which is slightly lighter than modern seawater (-0.83 ± 0.1‰, Foster et al., 2010; Ling et al., 2011). The δ^{26}Mg of the total high-temperature hydrothermal Mg sink should be equal to that of seawater since removal of Mg is quantitative in high-temperature hydrothermal systems (Tipper et al., 2006; Higgins and Schrag, 2010). By assuming a steady-state Mg isotopic composition for the oceans, the isotopically light riverine input has to be balanced by the combined removal of Mg through deposition of carbonates and low-temperature alteration. Thus, the behavior of Mg isotopes during low-temperature alteration of the oceanic crust is crucial to understanding Mg cycle in the oceans. However, this is still poorly known.

Knowledge of the Mg isotopic composition of the AOC can also provide valuable insight into the role of subduction in creating chemical heterogeneity in the mantle. Previous Mg isotopic measurements of global peridotite xenoliths and oceanic basalts led to the inference of a homogenous Mg isotopic composition of the mantle (-0.25 ± 0.07‰, Teng et al., 2010a). However, other mantle and mantle-derived rocks, including metasomatized mantle xenoliths (Pogge von Strandmann et al., 2011; Xiao et al., 2013; Hu et al., 2016b), continental basalts (Yang et al., 2012; Huang et al., 2015b; Liu et al., 2015; Tian et al., 2016; Li et al., 2017; Su et al., 2017) and cratonic eclogites (Wang et al., 2012, 2015; Huang et al., 2016) commonly have relatively low δ^{26}Mg values (-0.38 ± 0.23‰). These distinct Mg isotopic signatures are proposed to derive from AOC and marine sediment subduction into the mantle. This interpretation was supported by a first-order mass balance calculation showing that the bulk AOC has lighter Mg isotopic compositions than the unaltered oceanic crust (Teng et al., 2010b). However, recent studies of altered oceanic basalts recovered from IODP Sites 1256 (Huang et al., 2015a), U1365, U1367, and U1368 (Zhong et al., 2017) support a bulk AOC with Mg isotopic composition similar to or slightly heavier than that of the mantle. The contradiction between the mass balance approach and actual measurements of the Mg isotopic composition of the AOC has become a stumbling block in our understanding of the global Mg cycle.

In order to provide clarity to this conundrum, we present new Mg isotopic measurements of AOC samples recovered from the Ocean Drilling Program (ODP) Hole 801C outboard of the Mariana trench in the western Pacific (Fig. 1). This site offers some benefits in evaluating the elemental and isotopic effects of low temperature seafloor alteration and the potential influence of AOC subduction on mantle geochemistry. The reasons are twofold: (1) this site is in the oldest oceanic crust of the Pacific (~170 Ma, Koppers et al., 2003) and has undergone a full history of low-temperature alteration (Alt and Teagle, 2003); (2) this site lies in the fast spreading crust of the subducting Pacific

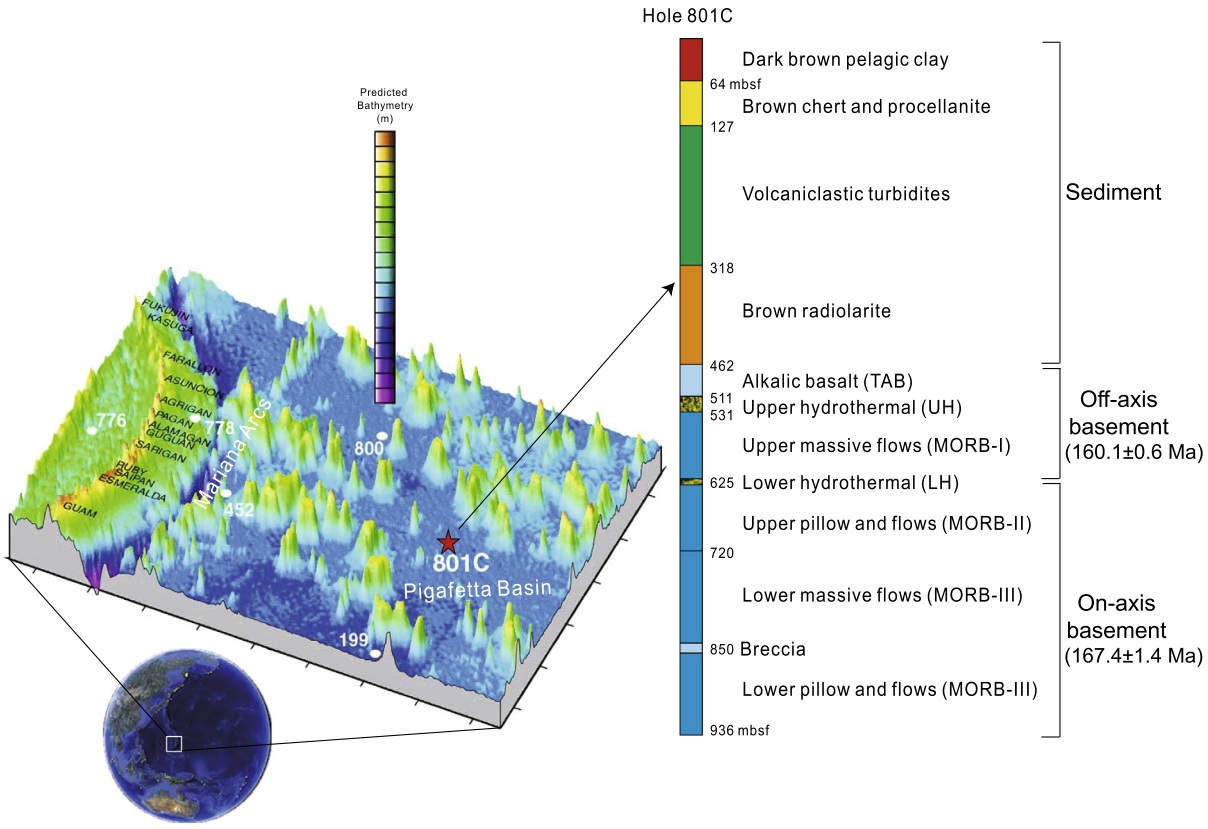

Fig. 1. Perspective map of ODP Hole 801C seaward of Mariana convergent margin and lithological variations of the oceanic crust recovered at this Site (revised from Plank et al., 2000). The ages of the on-axis and the off-axis basement are from Koppers et al. (2003).

plate (Bartolini and Larson, 2001) and has served as a geochemical reference site for the composition of subducting AOC (Plank et al., 2000; Kelley et al., 2003). Our results show that formation of secondary minerals during low-temperature alteration of the oceanic crust leads to Mg enrichments as well as large Mg isotope fractionation. Thus, subduction of the isotopically heterogeneous AOC, along with marine sediments, could produce mantle Mg isotopic heterogeneity.

2. GEOLOGICAL SETTINGS, ALTERATION HISTORY AND SAMPLES

ODP Site 801 is located at 18°38.538′N and 156° 21.588′E in the Pigafetta Basin outboard of the Mariana trench in the western Pacific Ocean (Plank et al., 2000) (Fig. 1). This site was first cored to 594 m below seafloor (mbsf) during ODP Leg 129 in 1989 and was extended to 935.7 mbsf during ODP Leg 185 in 1999, with a total basement penetration of 474 m and an average recovery rate of 47% (Plank et al., 2000).

The basement at Site 801 can be divided into six major units from top to bottom (Kelley et al., 2003) (Fig. 1): (1) the uppermost basement, a ~60-m-thick transitional/alkali basalt (TAB, 462–511 m below seafloor (mbsf)); (2) a ~20-m-thick upper hydrothermal layer (UH) with high apparent bulk porosity (~15%) at 511–531 mbsf; (3) the underlying ~100-m-thick MORB-I unit at 531–625 mbsf, consisting mainly of massive flows with minor thin flows and pillows; (4) a lower Si-Fe-rich hydrothermal layer (LH) below the MORB-I unit at 625 mbsf; (5) the MORB-II unit at 625–720 mbsf, characterized by tholeiitic pillows and flows with thin intervals of recrystallized sediments; (6) the MORB-III unit, including a massive flow unit (720–850 mbsf) and a series of thin (<1 m) sheet flows and pillows (850–936 mbsf). Both are separated by a tectonic breccia at 850 mbsf. The basaltic basement is overlain by a 462-m-thick sedimentary section (Fig. 1).

According to Ar geochronology, Koppers et al. (2003) suggested that the oceanic crust at Site 801 was formed in two stages: the section below 625 mbsf (MORB-II and MORB-III) were formed at the ridge at 167.4 ± 1.4 Ma, and the crust above 625 mbsf (TAB and MORB-I) were formed off-axis at 160.1 ± 0.6 Ma (Fig. 1). The 7.3 Myr gap between the sections above and below 625 mbsf indicates that the upper 175 m oceanic crust (MORB-I and TAB) intruded as sills close to the base of the accumulated sediments, and formed the upper hydrothermal layer (UH) (Koppers et al., 2003). Throughout this paper, we distinguish the off-axis basement (TAB and MORB-I) from the basement inferred to represent on-axis oceanic crust (MORB-II and MORB-III), with the boundary between them marked by the lower hydrothermal layer at 625 mbsf (Fig. 1).

2.1. Alteration history

The entire basement at Site 801 has undergone extensive low-temperature alteration and secondary mineralization (Alt et al., 1992; Alt and Teagle, 2003; Talbi and Honnorez, 2003; Alt, 2004). The principal secondary minerals are saponite (a Mg-rich Fe^{2+} smectite), celadonite (an Fe^{3+} mica), Fe-oxy-hydroxides, calcite and pyrite, all typical of low-temperature alteration (Alt and Teagle, 2003; Talbi and Honnorez, 2003). The temperature of alteration, estimated from the oxygen isotopic compositions of phyllosilicates and calcite, is between 10 °C and 95 °C and generally increases downward (Alt and Teagle, 2003).

The alteration at Site 801 falls into at least four categories, on the basis of secondary mineralogy (Plank et al., 2000; Alt and Teagle, 2003): (1) dark grey altered basalt, the most common alteration type throughout the basement, characterized by saponite and minor calcite replacing olivine; (2) dark alteration halos, the earliest stages of vein-related alteration, resulting from the replacement of olivine by celadonite and Fe-oxyhydroxides. This type of alteration is linked to distal hydrothermal fluids (Alt, 2004); (3) brown alteration halos, characterized by replacement of olivine by smectite and the presence of abundant Fe-oxyhydroxides disseminated in the groundmass; (4) pale green alteration in highly altered basalt, resulting from intense recrystallization to celadonite, smectite, glauconite, calcite, K-feldspar and titanite. This alteration type is commonly associated with hydrothermal silica-iron deposits.

Consequently, several successive alteration stages are identified in the AOC at Site 801 (Talbi and Honnorez, 2003; Alt, 2004). Celadonite is the earliest phase to form in dark alteration halos by low-temperature hydrothermal fluids. Iron-oxyhydroxides subsequently form in brown alteration halos by oxidized seawater solutions. Saponite and pyrite then pervasively form as condition become more reducing, and finally carbonates precipitate as fracture filling (Alt, 2004).

2.2. Samples

The AOC samples investigated here include 16 individual samples and 14 composite samples from Site 801C, all aliquots of the same powders analyzed in previous studies (e.g., Ludden et al., 2006).

(1) Individual samples: These 16 individual samples can be subdivided into three groups: (i) FLO samples, which are mainly composited of minimally altered basalt with small calcite or smectite veins; (ii) VCL samples, which mainly consist of breccia and hyaloclastites; (iii) IFM samples, which are interflow sediments filling the spaces between basalt pillows.
(2) Composite samples: The 14 composite samples analyzed here were generated from physical mixtures of 117 individual samples, weighted according to their proportions in the core (Kelley et al., 2003). Composite samples offer an efficient way to geochemically characterize large crustal section with a small number of analyses. Three types of composites have been made from each of the four basement units (TAB, MORB-I, MORB-II and MORB-III). The FLO composites were prepared from pillow lavas and massive flows at each unit. The VCL composites consist of highly altered volcanoclastic breccias and interflow sediments at each unit. The MIX composites are made up of 30% VCL and 70% FLO at each unit. In addition, a super-composite (SUPER) of the entire MORB basement was generated by combining the three MORB depth composites according to their respective thicknesses, and a sediment composite (SED) was made from the IFM from the upper 230 m of the basement (Alt, 2003b; Kelley et al., 2003).

3. ANALYTICAL METHODS

Approximately 1–5 mg of whole-rock powders were dissolved in a mixture of Optima-grade HF-HNO_3-HCl in Savillex screw-top beakers in order to obtain ~50 μg Mg for high-precision isotopic analysis. Magnesium was purified through two sets of columns. The first column contained Bio-Rad AG50W-X12 resin (200–400 mesh) and Mg was separated from Ca in 12 N HCl media, following previously established procedures (Ling et al., 2013; Huang et al., 2015c). This column procedure was repeated to completely separate Ca from Mg. The eluted Mg solution was dried down and then loaded onto a second column containing Bio-Rad AG50W-X8 resin (200–400 mesh), following established procedures (Yang et al., 2009; Li et al., 2010; Teng et al., 2010a). The second column procedure was also repeated in order to completely separate Mg from other matrix elements, in particular Na, K, Al and Fe. At least two standards were processed along with samples for each batch of column chemistry.

Magnesium isotope measurements were performed on the Nu Plasma multi-collector inductively coupled plasma mass-spectrometer (MC-ICP-MS) by the sample-standard bracketing method. The three Mg isotopes (24, 25 and 26) were measured simultaneously in separate Faraday cups in low-resolution mode, and no molecular interferences or doubly-charge interferences were observed (Teng and Yang, 2014). Magnesium isotopic data are presented in delta notation in per mil (‰) relative to a pure Mg standard solution DSM3:

$$\delta^{x}\mathrm{Mg}(‰) = \left[\left(^{x}\mathrm{Mg}/^{24}\mathrm{Mg}\right)_{\mathrm{sample}} / \left(^{x}\mathrm{Mg}/^{24}\mathrm{Mg}\right)_{\mathrm{DSM3}} - 1\right] \times 1000 \quad (1)$$

where x refers to either mass 25 or 26. At least one standard each session was analyzed as an unknown to evaluate accuracy and reproducibility. The δ^{26}Mg values of two in-house standards (Kilbourne Hole olivine and Hawaii seawater) and three USGS standards (BHOV-2, MAG-1, and SCo-1) analyzed during the course of this study are consistent with published data (Teng et al., 2015, and references therein) (Table 1).

Table 1
Magnesium isotopic compositions of reference materials analyzed in this study, and comparison with literature data.

Standard	Type	δ^{26}Mg	2SD	δ^{25}Mg	2SD	Reference
Hawaii seawater	Seawater	−0.86	0.09	−0.46	0.07	This study
Replicate		−0.83	0.07	−0.43	0.06	This study
Replicate		−0.81	0.07	−0.43	0.08	This study
Weight Average ($n = 3$)		−0.83	0.04	−0.44	0.04	This study
		−0.83	0.09	−0.43	0.06	Ling et al. (2011)
Kilbourne Hole Olivine	Olivine	−0.29	0.07	−0.13	0.05	This study
Duplicate		−0.25	0.06	−0.11	0.05	This study
Replicate		−0.22	0.07	−0.11	0.07	This study
Weight Average ($n = 3$)		−0.25	0.04	−0.12	0.03	This study
		−0.27	0.07	−0.14	0.04	Teng et al. (2010a)
BHVO-2	Basalt	−0.17	0.07	−0.11	0.05	This study
		−0.24	0.06	−0.12	0.05	Pogge von Strandmann et al. (2011)
		−0.14	0.08	−0.06	0.04	Wiechert and Halliday (2007)
SCO-1	Shale	−0.84	0.06	−0.44	0.04	This study
		−0.81	0.07			Wimpenny et al. (2014)
		−0.94	0.08	−0.5	0.06	Li et al. (2010)
MAG-1	Marine mud	−0.24	0.06	−0.07	0.06	This study
		−0.23	0.09	−0.14	0.04	Wombacher et al. (2009)

a. 2SD = 2 times the standard deviation of the population of n ($n > 20$) repeat measurements of the standards during an analytical session.
b. Replicate = repeat column chemistry and instrumental measurement of different aliquots of the same stock solution.
c. Duplicate = repeated measurement of Mg isotopic ratios on the same purified solutions.

4. RESULTS

The Mg concentrations and isotopic compositions of the individual and composite AOC samples are reported in Table 2 and plotted in Fig. 2.

The MgO concentration in unaltered basaltic glass from Site 801 varies from 5.9 to 9.3 wt% (Fisk and Kelley, 2002). In comparison, the AOC samples have a larger range in MgO, varying from 1.6 to 15.6 wt%. MgO contents of the individual AOC samples vary between 1.6 and 9.0 wt% in

Table 2
Descriptions, major elemental contents and Mg isotopic compositions of composite and individual AOC samples recovered from ODP Hole 801C.

Sample ID	Type of alteration	Depth (mbsf)	MgO (wt.%)	$(Mg/Ti)_{norm}$	FeO^*/CaO	$\delta^{26}Mg \pm 2SD$	$\delta^{25}Mg \pm 2SD$
Composite sample							
801C-TAB-FLO	FLO	487.00	5.84	0.57	1.03	−0.54 ± 0.07	−0.26 ± 0.05
Replicate						−0.53 ± 0.06	−0.29 ± 0.04
Average						−0.53 ± 0.05	−0.28 ± 0.03
801C-TAB-VCL	VCL	487.00	5.77	1.19	0.51	−0.99 ± 0.07	−0.49 ± 0.08
Replicate						−1.03 ± 0.07	−0.53 ± 0.08
Average						−1.01 ± 0.05	−0.51 ± 0.05
801C-TAB-MIX	MIX	487.00	5.71	0.67	0.85	−0.68 ± 0.07	−0.34 ± 0.08
Replicate						−0.68 ± 0.06	−0.37 ± 0.04
Average						−0.68 ± 0.05	−0.37 ± 0.04
801C-MORB I-FLO	FLO	575.00	5.37	0.60	0.72	−0.22 ± 0.07	−0.11 ± 0.08
Replicate						−0.19 ± 0.07	−0.09 ± 0.05
Average						−0.21 ± 0.05	−0.10 ± 0.04
801C-MORB I-VCL	VCL	575.00	4.51	0.96	0.56	−0.46 ± 0.09	−0.24 ± 0.07
Replicate						−0.43 ± 0.07	−0.20 ± 0.05
Average						−0.44 ± 0.05	−0.22 ± 0.04
801C-MORB I-MIX	MIX	575.00	5.28	0.67	0.66	−0.23 ± 0.07	−0.14 ± 0.05
Replicate						−0.23 ± 0.07	−0.13 ± 0.08
Average						−0.23 ± 0.05	−0.14 ± 0.04
801C-MORB II-FLO	FLO	680.50	6.62	0.87	0.99	−0.19 ± 0.06	−0.10 ± 0.05
Replicate						−0.13 ± 0.06	−0.06 ± 0.04
Average						−0.16 ± 0.04	−0.08 ± 0.03
801C-MORB II-VCL	VCL	680.50	6.02	1.58	0.70	0.12 ± 0.07	0.04 ± 0.05
Replicate						0.17 ± 0.06	0.09 ± 0.04
Average						0.15 ± 0.05	0.07 ± 0.03

(*continued on next page*)

Table 2 (*continued*)

Sample ID	Type of alteration	Depth (mbsf)	MgO (wt.%)	$(Mg/Ti)_{norm}$	FeO^*/CaO	$\delta^{26}Mg \pm 2SD$	$\delta^{25}Mg \pm 2SD$
801C-MORB II-MIX	MIX	680.50	6.56	1.00	0.90	0.00 ± 0.07	0.00 ± 0.05
Replicate						−0.02 ± 0.06	−0.02 ± 0.04
Average						−0.02 ± 0.06	−0.02 ± 0.04
801C-MORB III-FLO	FLO	839.50	6.73	1.00	1.21	−0.04 ± 0.07	−0.01 ± 0.05
Replicate						0.00 ± 0.06	0.04 ± 0.04
Average						−0.04 ± 0.07	0.02 ± 0.03
801C-MORB III-VCL	VCL	839.50	7.61	1.45	1.38	0.10 ± 0.09	0.06 ± 0.07
Replicate						0.13 ± 0.06	0.06 ± 0.05
Average						0.12 ± 0.05	0.06 ± 0.04
801C-MORB III-MIX	MIX	839.50	6.98	1.09	1.24	0.05 ± 0.07	0.03 ± 0.05
Replicate						0.03 ± 0.06	0.04 ± 0.04
Average						0.04 ± 0.05	0.04 ± 0.03
801C-SUPER	SUPER		6.35	0.96	0.95	−0.03 ± 0.09	−0.02 ± 0.07
Replicate						−0.02 ± 0.07	−0.01 ± 0.08
Average						−0.02 ± 0.06	−0.02 ± 0.05
801C-SED	SED		2.67		0.45	−1.37 ± 0.09	−0.68 ± 0.06
Replicate						−1.34 ± 0.06	−0.71 ± 0.05
Average						−1.35 ± 0.05	−0.71 ± 0.04
Individual sample							
801C-5R3-80-81	FLO	534.55	1.57	0.29	0.38	−1.68 ± 0.06	−0.88 ± 0.05
Replicate						−1.72 ± 0.06	−0.90 ± 0.05
Replicate						−1.70 ± 0.06	−0.89 ± 0.07
Average						−1.70 ± 0.03	−0.89 ± 0.03
801C-10R2-72-77	FLO, pillow-breccia	571.22	7.36	1.09	0.94	−0.02 ± 0.06	0.01 ± 0.05
Replicate						−0.05 ± 0.06	0.02 ± 0.06
Average						−0.04 ± 0.04	0.01 ± 0.04
801C-14R2-117-120	Interflow material (IFM)	606.48	15.60		0.31	−0.34 ± 0.06	−0.18 ± 0.05
Replicate						−0.37 ± 0.06	−0.19 ± 0.05
Replicate						−0.36 ± 0.06	−0.14 ± 0.06
Average						−0.35 ± 0.03	−0.17 ± 0.03
801C-16R2-82-86	FLO, pillow-breccia	625.56	2.79	0.41	0.60	−0.09 ± 0.07	−0.04 ± 0.05
Replicate						−0.07 ± 0.06	−0.04 ± 0.05
Average						−0.08 ± 0.05	−0.04 ± 0.04
801C-17R4-15-18	Interflow breccia (IFM)	637.37	4.31		0.51	−0.03 ± 0.07	−0.02 ± 0.07
Replicate						0.04 ± 0.09	−0.05 ± 0.07
Replicate						−0.06 ± 0.09	−0.01 ± 0.06
Average						−0.02 ± 0.05	−0.03 ± 0.04
801C-21R2-69-71	Interflow calcite (IFM)	672.12	1.48		0.03	−2.73 ± 0.09	−1.48 ± 0.07
Replicate						−2.78 ± 0.09	−1.47 ± 0.07
Replicate						−2.76 ± 0.09	−1.43 ± 0.06
Average						−2.76 ± 0.05	−1.46 ± 0.04
801C-24R2-116-120	VCL, breccia	693.79	9.16	1.61	2.60	0.16 ± 0.07	0.08 ± 0.06
Duplicate						0.15 ± 0.06	0.09 ± 0.05
Replicate						0.15 ± 0.06	0.11 ± 0.06
Average						0.15 ± 0.04	0.09 ± 0.03
801C-27R3-66-69	FLO, massive basalt	723.14	6.07	0.79	0.80	−0.07 ± 0.06	−0.02 ± 0.06
801C-30R1-111-114	FLO, massive basalt	748.41	6.43	0.95	1.25	−0.18 ± 0.06	−0.1 ± 0.05
Replicate						−0.12 ± 0.06	−0.04 ± 0.07
Average						−0.15 ± 0.04	−0.08 ± 0.04
801C-31R4-43-45	FLO, massive basalt	761.02	6.20	0.90	1.21	−0.18 ± 0.09	−0.08 ± 0.07
Replicate						−0.15 ± 0.06	−0.07 ± 0.06
Average						−0.16 ± 0.05	−0.07 ± 0.05
801C-31R7-7-10	FLO, massive basalt	764.81	8.19	1.30	1.70	0.18 ± 0.07	0.12 ± 0.06
Duplicate						0.20 ± 0.06	0.08 ± 0.05
Replicate						0.24 ± 0.06	0.18 ± 0.06
Average						0.21 ± 0.04	0.12 ± 0.03
801C-36R3-87-90	VCL, breccia	807.64	4.72	1.10	1.78	−0.05 ± 0.07	−0.03 ± 0.06
Replicate						−0.02 ± 0.06	−0.01 ± 0.07
Average						−0.03 ± 0.05	−0.02 ± 0.05
801C-37R5-112-114	FLO, massive basalt	819.58	9.01	1.80	2.73	0.18 ± 0.07	0.09 ± 0.06
Duplicate						0.19 ± 0.06	0.13 ± 0.05
Replicate						0.21 ± 0.06	0.14 ± 0.07
Average						0.20 ± 0.04	0.12 ± 0.03

(*continued on next page*)

Table 2 (*continued*)

Sample ID	Type of alteration	Depth (mbsf)	MgO (wt.%)	$(Mg/Ti)_{norm}$	FeO^*/CaO	$\delta^{26}Mg \pm 2SD$	$\delta^{25}Mg \pm 2SD$
801C-38R3-53-59	VCL, breccia	826.29	10.15	1.36	2.79	0.17 ± 0.06	0.07 ± 0.05
Replicate						0.11 ± 0.06	0.08 ± 0.07
Average						0.14 ± 0.04	0.07 ± 0.04
801C-40R1-24-27	VCL, breccia	841.74	6.37	1.36	0.43	0.19 ± 0.07	0.12 ± 0.05
Replicate						0.18 ± 0.06	0.07 ± 0.07
Average						0.18 ± 0.05	0.10 ± 0.04
801C-43R1-13-15	FLO, massive basalt	869.23	6.77	1.03	1.08	−0.14 ± 0.06	−0.06 ± 0.07

Depth, major element concentration are from Kelley et al. (2003).
a. mbsf = meter below sea floor.
b. 2SD = 2 times the standard deviation of the population of n ($n > 20$) repeat measurement of the standards during an analytical session.
c. Replicate = repeat column chemistry and instrumental measurement of different aliquots of the same stock solution.
d. Duplicate = repeat instrumental measurement of the same purified Mg solution.
e. FLO = less altered basaltic flows; VCL = highly altered breccias and volcaniclastics; MIX = 30% VCL + 70% FLO; SUPER = composite of the whole MORB basement; SED = composite of interflow sediments in the upper 230 m of the section.

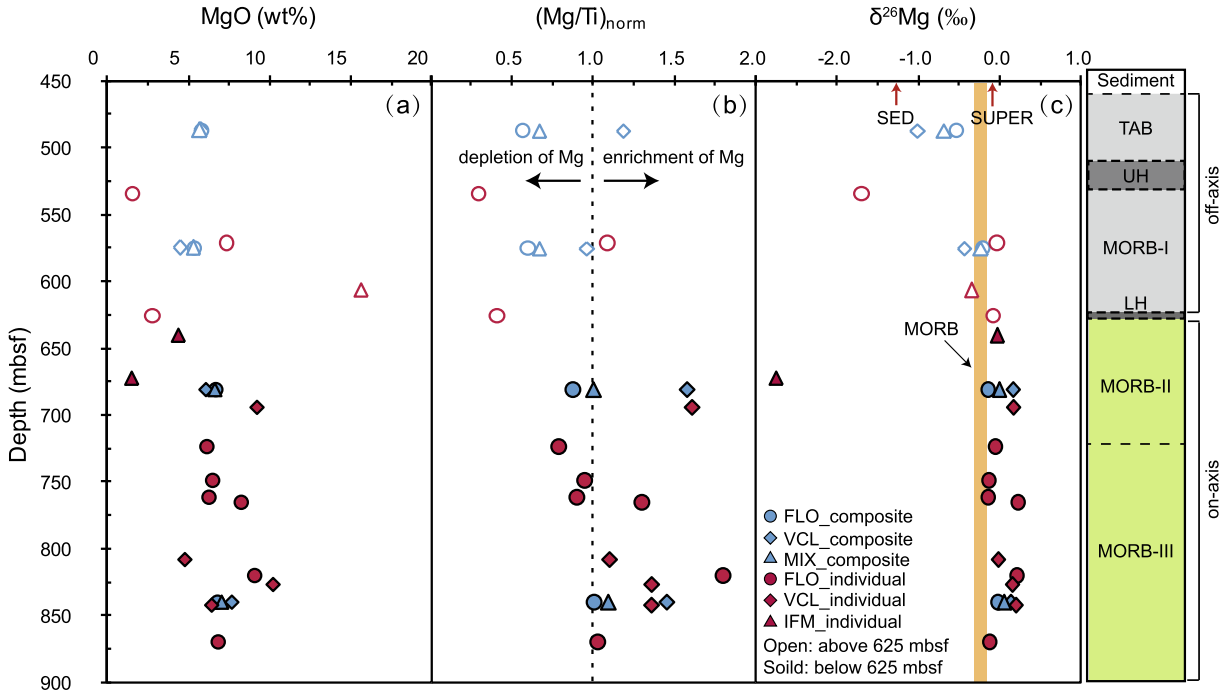

Fig. 2. Downhole variation of (a) MgO concentration, (b) Mg/Ti normalized ratio and (c) $\delta^{26}Mg$ of individual and composite AOC samples at Site 801. $Mg/Ti_{norm} > 1$ reflects net addition of Mg from the AOC, while values < 1 reflect net Mg depletion (see text for the definition and calculation of Mg/Ti_{norm}). The vertical yellow bar in panel c and in the following figures represents the $\delta^{26}Mg$ range of fresh MORB (−0.25 ± 0.07‰, Teng et al., 2010a). Shown on the right is the stratigraphic section for the altered oceanic crust at Site 801. "UH" and "LH" refers to the upper and lower hydrothermal deposits, respectively. Open and solid symbols in this figure and the following ones refer to off-axis samples and on-axis samples, respectively. (For interpretation of the references to colour in this figure legend, the reader is referred to the web version of this article.)

FLO-type, between 4.7 and 10.2 wt% in VCL-type, and between 1.5 and 15.6 wt% in IFM-type, respectively. By contrast, MgO contents of the composites vary less, from 4.4 to 7.5 wt% (Fig. 2). VCL composites span a larger range in MgO (4.5 to 7.6 wt%) than the FLO composites (5.4 to 6.7 wt%) (Fig. 2a), and the MIX composites have intermediate MgO contents ranging between 5.3 wt% and 7.0 wt%. The SUPER composite has a MgO content of 6.4 wt%, whereas the SED composite has a lower MgO content of 2.7 wt%.

Similar to MgO concentrations, $\delta^{26}Mg$ values of the individual AOC samples exhibit a large variation, ranging from −2.76‰ to 0.21‰, and are on average heavier than the fresh MORB (−0.25 ± 0.07‰, Teng et al., 2010a) (Table 2). In detail, $\delta^{26}Mg$ values of the individual FLO and VCL samples vary from −1.70‰ to 0.21‰, and from

−0.03‰ to 0.18‰, respectively (Table 2). Most of the individual IFM samples (14R2, 17R4 and 21R2) have δ^{26}Mg values lower than the fresh MORB, ranging between −2.76‰ to −0.02‰ (Table 2).

The δ^{26}Mg values of the composite samples vary from −0.53‰ to −0.04‰ in FLO-type, and from −1.01‰ to 0.15‰ in VCL-type (Table 2). The MIX composites have δ^{26}Mg values (−0.68‰ to 0.04‰) intermediate between the FLO and VCL composites in the same depth interval (Fig. 2c). The SUPER composite has δ^{26}Mg value of −0.02‰, notably higher than that of fresh MORB (Fig. 2c). The SED composite has a δ^{26}Mg value of −1.39‰, which is much lower than fresh MORB and modern seawater (−0.83 ± 0.1‰, Ling et al., 2011).

Collectively, the δ^{26}Mg values of the individual and composite samples increase with depth (Fig. 2c). Apart from the IFM samples, AOC from the lower on-axis basement below 625 mbsf (MORB-II and -III) have higher δ^{26}Mg (−0.16‰ to 0.20‰) than the fresh MORB, whereas δ^{26}Mg values (−1.7‰ to −0.04‰) of AOC samples from the upper off-axis basement (TAB and MORB-I) are significantly lower than the fresh MORB (Fig. 2c).

5. DISCUSSION

In this section, we first discuss the changes in Mg concentration and Mg isotopes during low-temperature alteration of the oceanic crust, and then use our data to estimate the average Mg isotopic composition of the altered oceanic crust. Finally, we explore the implications of our results on cycling of Mg in the oceans and Mg isotopic heterogeneity in the mantle.

5.1. The change of MgO due to low-temperature alteration of the oceanic crust

Approximately one third of the heat loss from the Earth's interior through formation of new oceanic crust is removed by seawater circulation at the ridge axis and on the ridge flank (Coggon and Teagle, 2011). During this process, primary minerals are progressively dissolved and secondary minerals are deposited due to reaction with circulating fluids, altering both the chemistry of the fluid and the rock. Large changes in the composition of the circulating seawater are generally produced during high-temperature hydrothermal circulation at the ridge axis, whereas small changes are produced by low-temperature circulation through ridge flank and hence difficult to quantify (Alt, 2003a; Staudigel, 2014).

Two approaches have been used to assess the chemical changes due to low-temperature alteration of the oceanic crust on the ridge flank. One is based on the change in the composition of seawater circulating through basement, which is in turn inferred from profiles of sediment porewater chemistry (e.g., Mottl and Wheat, 1994). The other uses chemical differences between fresh and altered rocks expressed as global fluxes via oceanic crust production rates (e.g., Staudigel et al., 1996). Previous studies on the compositions of sediment porewaters and low-temperature hydrothermal fluids demonstrated that low-temperature alteration of the oceanic crust removed Mg from seawater and serves as an additional Mg sink to balance the excess Mg input to the oceans (Kastner and Gieskes, 1976; Mottl and Wheat, 1994; Elderfield et al., 1999). However, there is considerable variation in the composition of altered and fresh samples in drilled sections of upper oceanic crust. For example, ODP Site 504B indicates a net uptake of Mg from seawater (Alt et al., 1996), whereas Sites 417/418 and 801 show either no change or a slight loss of Mg to seawater (Staudigel et al., 1996; Kelley et al., 2003). The lack of an obvious enrichment of Mg in bulk altered oceanic basalts may result from small losses of Mg-bearing material during coring (Nielsen et al., 2006), or from the large uncertainties in normalizating AOC to fresh glasses (Kelley et al., 2003). These uncertainties derive from both the large variation that may be present in the MgO concentration of fresh glasses (as at ODP site 801) and in the dilution of MgO during alteration by other components (e.g., H_2O, $CaCO_3$, SiO_2).

We use a modified approach to re-evaluate the net change in Mg due to low-temperature alteration of the oceanic crust at Site 801. To evaluate the relative depletion or enrichment of Mg during seafloor alteration, we use a reference immobile element Ti (MacLean and Barrett, 1993) and the following equation:

$$(Mg/Ti)_{norm} = (MgO/TiO_2)_{AOC}/(MgO/TiO_2)_{Fresh} \quad (2)$$

where $(MgO/TiO_2)_{AOC}$ and $(MgO/TiO_2)_{Fresh}$ refer to Mg/Ti ratio of altered oceanic basalt and fresh oceanic basalt, respectively. $(Mg/Ti)_{norm} > 1$ reflects addition of Mg and $(Mg/Ti)_{norm} < 1$ reflects depletion.

This calculation requires first estimating the MgO/TiO_2 ratio of the fresh basalt protolith for each sample. However, $(MgO/TiO_2)_{Fresh}$ varies substantially in our samples because Ti is an incompatible element that increases in concentration as MgO decreases in concentration during fractional crystallization of MORB (as in the basalt glass trend in Fig. 3b) (Klein, 2003). We thus use Ni-TiO_2 systematic to ascertain the overall level of igneous evolution experienced by each sample (Fig. 3a), because neither of these elements appears to be significantly affected by alteration (Humphris and Thompson, 1978; MacLean and Barrett, 1993). This is apparent given that the freshest samples plot on the fractionation curve of basalt glass, and the most altered samples plot towards the origin in Fig. 3a. The intersection of the sample's Ni/TiO_2 with the fractionation curve of basalt glass provides the fresh TiO_2 content of each sample (Fig. 3a). The fresh TiO_2 content then yields the fresh MgO content and MgO/TiO_2 ratio based on the basalt glass trend in Fig. 3b. It would be simpler to compare the MgO/Ni of the AOC to that in the fresh basaltic glass, but few glass samples have both MgO and Ni data. Critical to this approach is the assumption that the basalt glass trend (based on the preservation of fresh glass in these ancient basalts, Fisk and Kelley, 2002) is the same as the fresh whole rock trend. This is true provided the crystal content of the whole rock is low (Plank et al., 2000), which is generally the case for MORB (Gale et al., 2013).

We use the composition of sample 37R as an example calculation of $(Mg/Ti)_{norm}$. Its Ti and Ni concentrations

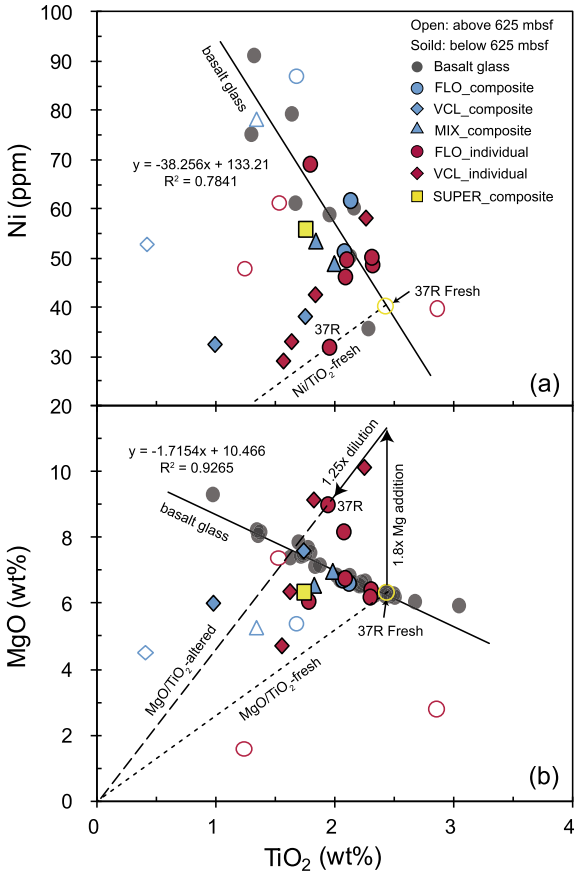

Fig. 3. Plots of (a) Ni and (b) MgO versus TiO_2 concentrations for individual AOC samples, composites and basalt glass samples at Site 801. The solid lines labeled with "basalt glass" are regressions lines fit through the basalt glass data (from Kelley et al., 2003). Dashed lines are lines of constant ratio. An example calculation of Mg/Ti_{norm} is illustrated for sample 37R, which has a Mg/Ti_{norm} value of 1.8, reflecting a factor of 1.8 enrichment in Mg, consistent with the abundance of saponite in this sample. Note that IFM samples and the sediment composite (SED) are not plotted here nor used to calculated Mg/Ti_{norm} since they are mostly composed of precipitates with low TiO_2 content (<0.1 wt%) and not basaltic material.

are shifted toward the origin and below the fresh glass array in Fig. 3a, reflecting the dilution effect during alteration. If the Ni/TiO_2 ratio of 37R is projected to the glass array, then its fresh TiO_2 content is 2.4 wt%. Such a high TiO_2 content is consistent with the sample's low Ni/TiO_2, indicating it has experienced a great amount of crystal fractionation. A fresh TiO_2 content of 2.4 wt% yields a fresh MgO content of 6.3 wt%, if the composition of 37R is constrained to lie along the glass trend in Fig. 3b. When the altered MgO/TiO_2 ratio divided by the resulting fresh one, the $(Mg/Ti)_{norm}$ is 1.8, indicating strong Mg addition. The combined effects of 1.8 times addition and 1.25 times dilution by carbonates and other components lead to the altered MgO concentration of 9.0 wt% (Fig. 3b). The extreme Mg addition experienced by this sample is consistent with its abundant saponite veins (Table 2).

Our results show that $(Mg/Ti)_{norm}$ values < 1 are generally found in the off-axis basement above 625 mbsf, while most of the AOC samples from the on-axis basement below 625 mbsf have $(Mg/Ti)_{norm}$ values > 1 (Fig. 2b). The VCL samples, except those in the MORB-I composite, have $(Mg/Ti)_{norm} > 1$, implying addition of Mg to the AOC during low-temperature alteration. This is in agreement with Mg-addition characterizing alteration of the 'normal' oceanic crust, which is often inferred from pore water profiles (Mottl and Wheat, 1994). However, the SUPER composite, composed of the MORB-I, II and III sections with some SED material, has a $(Mg/Ti)_{norm}$ value of ~1 (Table 2), reflecting no significant net addition of Mg. Because the individual AOC samples show both Mg depletion (in MORB-I) and addition (in MORB-II and III), the $(Mg/Ti)_{norm} \sim 1$ of the SUPER composite is probably a coincidence. In sum, variability in the $(Mg/Ti)_{norm}$ values of AOC might be attributed to multi-stage alteration of the basement and the influence of interflow sediment in the off-axis basement.

5.2. Behavior of Mg isotopes during low-temperature alteration of the oceanic crust

Altered oceanic basalts recovered from Site 801 have variable $\delta^{26}Mg$ values (−1.70‰ to 0.21‰) with systemically heavier Mg isotopic compositions in the on-axis basement below 625 mbsf than in the overlain off-axis basement. Such large Mg isotopic variation is unlikely to result from isotopic heterogeneity of the pristine oceanic crust because unaltered oceanic basalts have homogenous Mg isotopic composition (-0.25 ± 0.07‰) owing to limited isotope fractionation during igneous processes (Teng et al., 2010a). More likely, these highly variable $\delta^{26}Mg$ values are produced by Mg isotope fractionation during seawater circulation through oceanic crust, accompanied by dissolution of primary igneous minerals and formation of secondary minerals.

5.2.1. Primary mineral dissolution cannot explain the Mg isotopic signatures

Experimental studies of silicate mineral dissolution demonstrate that conservative mixing of isotopically distinct Mg-bearing minerals and kinetic fractionation with preferential release of light Mg isotopes into solutions can produce Mg isotopic variation in leaching solutions (Wimpenny et al., 2010; Ryu et al., 2011). However, $\delta^{26}Mg$ variation in AOC cannot be explained by selective dissolution of Mg-bearing minerals, because Mg-bearing primary materials in fresh oceanic basalts (including pyroxene, olivine and basalt glass) have similar Mg isotopic composition (Handler et al., 2009; Teng et al., 2010a; Oeser et al., 2014; Hu et al., 2016a). Kinetic leaching of ^{24}Mg during primary mineral dissolution can also be excluded as it would lead to the enrichment of heavy Mg isotopes but depletion of MgO in the AOC, and hence a negative correlation between $\delta^{26}Mg$ and $(Mg/Ti)_{norm}$ (Wimpenny et al., 2010), which is opposite to what is observed here (Fig. 4). This cannot explain MgO enrichment with high $\delta^{26}Mg$ values in the on-axis basement below 625 mbsf (Fig. 2). Thus,

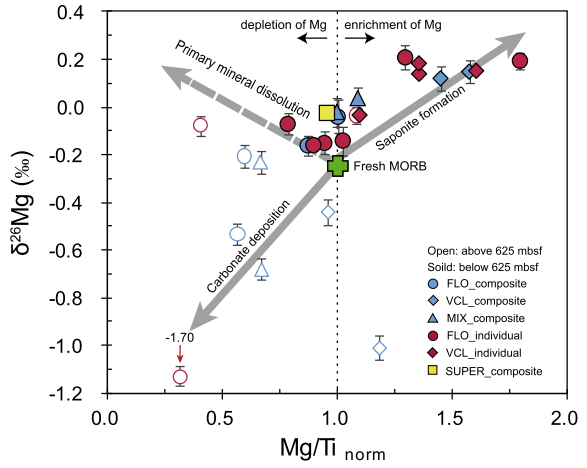

Fig. 4. Plot of δ^{26}Mg values and Mg/Ti_{norm} ratios in AOC samples. Green cross represents the average composition of fresh MORB ($\delta^{26}Mg = -0.25 \pm 0.07‰$, Teng et al., 2010a). (For interpretation of the references to colour in this figure legend, the reader is referred to the web version of this article.)

primary mineral dissolution is unlikely to be the principal cause of large Mg isotopic variation in the AOC at Site 801.

5.2.2. Secondary mineral formation accounts for the Mg isotopic variations

The AOC samples at Site 801 contain a typical low-temperature alteration assemblage of saponite, celadonite, palagonite, calcite, Fe-oxy-hydroxides and pyrite (Alt and Teagle, 2003; Talbi and Honnorez, 2003). Among these secondary minerals, ferrous saponite is the main host of Mg. Celadonite contains moderate Mg as well as appreciable potassium and ferric iron, while a relatively small amount of Mg is hosted in calcite (Seyfried et al., 1978; Talbi and Honnorez, 2003). The low abundance of celadonite (<10%) in veins throughout the basement (Plank et al., 2000; Alt and Teagle, 2003) together with the lack of correlation between MgO and K_2O contents in the AOC samples (Fig. 5a), indicate that celadonite is not the dominant Mg-bearing mineral in the AOC at Site 801. A positive correlation between the FeO* (total Fe) and MgO contents (Fig. 5b) and a negative correlation between the CaO and MgO contents of the AOC samples (Fig. 5c), suggest that the MgO contents are mainly controlled by the relative proportion of saponite and calcite. This is confirmed by the mixing lines between saponite and calcite with varying composition shown in Fig. 5, which encompass almost all of the AOC samples.

The highly variable δ^{26}Mg values observed in the AOC at Site 801 therefore most likely result from formation of secondary minerals. This is further endorsed by covariation of δ^{26}Mg and δ^{18}O in the on-axis and off-axis basement, as heavy oxygen isotopes are usually enriched in secondary minerals during alteration of the oceanic crust at temperatures lower than 250 °C (Muehlenbachs and Clayton, 1972; Staudigel et al., 1995). On the other hand, the opposite sense of the δ^{26}Mg and δ^{18}O correlations in the on-axis and off-axis samples demonstrates the different behavior

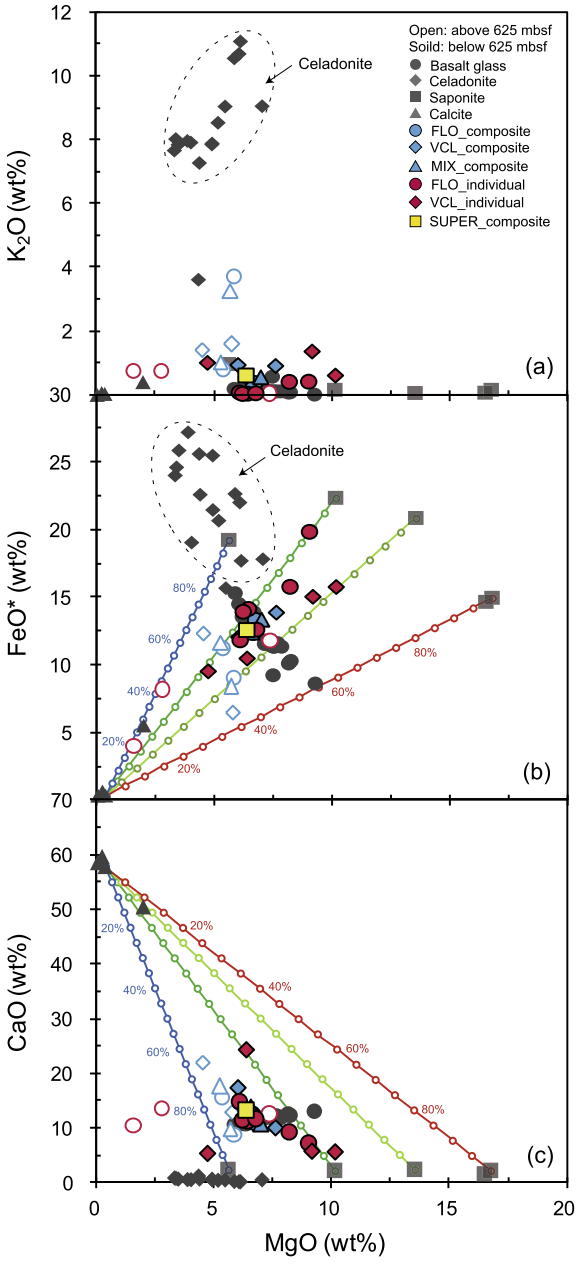

Fig. 5. Plots of MgO versus (a) K_2O, (b) FeO*, (c) CaO for the individual and composite AOC samples at Site 801. Major elemental data of AOC bulk samples and basalt glass are from Kelley et al. (2003), and secondary minerals separated from the AOC are from Talbi and Honnorez (2003). Colored solid lines are binary mixing lines between saponite and calcite of varying composition. The numbers along the mixing lines refer to the fractional contributions from these end-members. (For interpretation of the references to colour in this figure legend, the reader is referred to the web version of this article.)

of Mg isotopes during alteration in these two parts of basement (Fig. 6). Thus, these large Mg isotopic variations were produced by multi-stage alteration, with early formation of saponite accounting for high δ^{26}Mg in the lower basement, and subsequent precipitation of carbonates resulting in low δ^{26}Mg in the upper basement.

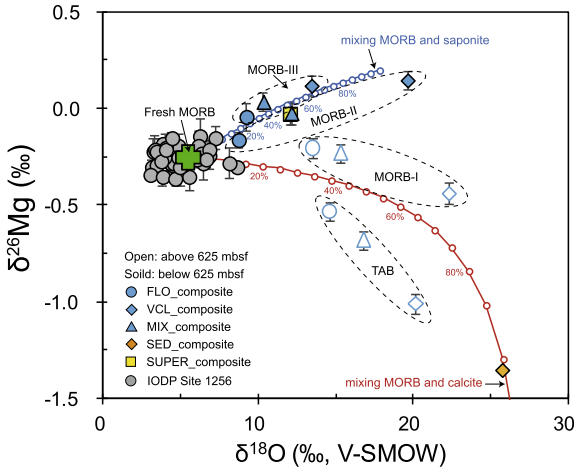

Fig. 6. Plot of $\delta^{26}Mg$ and $\delta^{18}O$ (relative to VSMOW) values for composite samples from Site 801. The $\delta^{18}O$ values of AOC composites are from Alt (2003), and the data of IODP Site 1256 are from Huang et al. (2015a). Green cross represents average composition of fresh MORB (5.5 ± 0.5‰, Cooper et al., 2009). The dotted solid lines are binary mixing lines between fresh MORB and saponite (blue line) and between unaltered MORB and calcite (red line). The numbers along the mixing lines refer to the fractional contributions from these end-members. (For interpretation of the references to colour in this figure legend, the reader is referred to the web version of this article.)

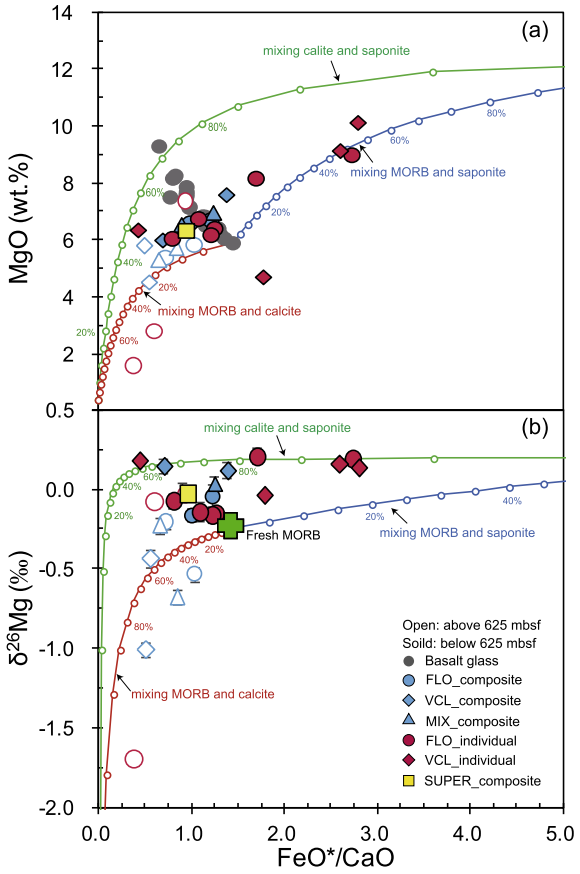

Fig. 7. (a) Plots of MgO versus FeO^*/CaO ratio of the individual and composite AOC samples at Site 801. Major elemental data are from Kelley et al. (2003). (b) Correlation between FeO^*/CaO ratio and $\delta^{26}Mg$ for individual and composite AOC samples at ODP Hole 801C. The dotted solid lines are binary mixing lines between fresh MORB and saponite (blue line), between unaltered MORB and calcite (red line), and between saponite and calcite (green line). Major elemental and isotopic compositions for the three end-members are: (1) saponite with FeO^*/CaO ratio of 8.84 and $\delta^{26}Mg$ of 0.20‰ (Ryu et al., 2016); (2) calcite with FeO^*/CaO ratio of 0.01 and $\delta^{26}Mg$ of −3.0‰ (Saulnier et al., 2012); (3) fresh basalt with FeO^*/CaO ratio of 1.46 and $\delta^{26}Mg$ of −0.25‰ ((Kelley et al., 2003; Teng et al., 2010a). The numbers along the mixing lines refer to the fractional contributions from these end-members. (For interpretation of the references to colour in this figure legend, the reader is referred to the web version of this article.)

5.2.2.1. The on-axis basement (below 625 mbsf). Petrographic studies of Site 801 samples found pervasive recrystallization to saponite, minor calcite, as well as disseminated pyrite in the on-axis basement, most likely due to replacement of olivine under low water/rock ratio, high pH and anoxic conditions (Plank et al., 2000; Alt and Teagle, 2003; Talbi and Honnorez, 2003). High abundance of saponite (up to 63%) in the on-axis basement may account for the enrichment of Mg (i.e., $(Mg/Ti)_{norm} > 1$), because both laboratory experiments (Seyfried and Bischoff, 1979) and field observations (Elderfield et al., 1999; Wheat and Fisher, 2008) demonstrate that Mg is removed from seawater by the formation of clay minerals during the seafloor alteration. Furthermore, a positive correlation between $\delta^{26}Mg$ and FeO^*/CaO (Fig. 7b) implies that heavy Mg isotopes are preferentially sequestered by the formation of saponite during the early stage of alteration, leading to the relatively high $\delta^{26}Mg$ and $(Mg/Ti)_{norm} > 1$ in the on-axis basement at Site 801 (Fig. 2). Additional support comes from the positive correlation between $\delta^{26}Mg$ and $(Mg/Ti)_{norm}$ of the AOC samples in this portion of the basement (Fig. 4), suggesting that heavy Mg isotopes are removed from seawater by the formation of clay minerals.

5.2.2.2. The off-axis basement (above 625 mbsf). In contrast to the on-axis AOC samples, the majority of AOC samples from the overlying off-axis basement (TAB and MORB-I) have relatively low $\delta^{26}Mg$ values with $(Mg/Ti)_{norm} < 1$ (Fig. 4), which most likely results from the addition of carbonates and concomitant dissolution of primary phases. Indeed, the off-axis basement has relatively higher abundance of carbonates than the on-axis basement (Alt and Teagle, 2003). This may ascribe to high intergranular porosity and permeability of the off-axis basement, which facilitate seawater penetration and oxidative alteration (Plank et al., 2000; Alt, 2003b). During this process, ferrous iron in basalt and pyrite are oxidized by O_2-rich seawater and generates H^+ (Seyfried et al., 1978), which, in turn, increases saponite solubility and results in a loss of heavy Mg isotopes and a depletion of Mg in the off-axis basement. Meanwhile, H^+ enhances dissolution of primary minerals in basalt and releases significant Ca^{2+} and Mg^{2+} into the pore water, which in turn accelerates precipitation of carbonates in veins (Fisher, 1998; Alt, 2003b). Moreover, high

atmospheric CO_2 levels in the Mesozoic may be conducive to carbonate precipitation in AOC (Staudigel et al., 1989; Alt and Teagle, 1999; Gillis and Coogan, 2011). Light Mg isotopes will be preferentially incorporated into calcite when precipitated from fluids (Saenger and Wang, 2014). A binary mixing calculation suggests that addition of 20% calcite could produce δ^{26}Mg in AOC of −0.30‰, but at least 60% of calcite is required to shift δ^{26}Mg of AOC to −0.50‰ (Fig. 7b). Such high amounts of calcite addition indicates an additional process may account for the extremely low δ^{26}Mg values (<−0.50‰).

Previous studies found that large quantities of interflow sediments were accumulated in the off-axis lavas by multiple sill intrusions (Koppers et al., 2003). These interflow sediments usually contain high abundance of carbonates (Alt and Teagle, 2003), with relatively light δ^{26}Mg and high δ^{18}O values. For example, the SED composite, consisting largely of such interflow sediments, has δ^{26}Mg of −1.35‰ and δ^{18}O of 25.70‰ (Table 2). Thus, accumulation of the carbonate-rich interflow sediments in the off-axis lavas could contribute to low δ^{26}Mg and high δ^{18}O values. This interpretation is further supported by an inverse correlation between δ^{18}O and δ^{26}Mg of the composites in the off-axis basement (Fig. 6).

5.3. Magnesium isotopic composition of the altered oceanic crust

Knowledge on the average composition of the heterogeneous AOC is important for understanding the chemical fluxes associated with oceanic crust alteration and global elemental cycling (Staudigel, 2014). Two approaches have been adopted to estimate the average chemical and isotopic compositions of the AOC (Staudigel et al., 1996; Kelley et al., 2003). One is to establish a weighted average of the compositions of a large number of individual rock samples throughout the basement. The other is to analyze a smaller set of composites, which themselves are weighted mixtures of many individual samples. Although information is lost on the internal structure of the oceanic crust as well as the heterogeneity at the scale of individual samples (Smith et al., 1995), composites provide an efficient way to obtain a complete geochemical characterization of a large crustal section with few analyses (Staudigel, 2003). Thus, we prefer to use composite samples to estimate the average Mg isotopic composition of the oceanic crust at Site 801.

The off-axis basement (TAB and MORB-I) has undergone a more complex alteration history and has more interflow sediments than normal oceanic crust. Thus, we use only the on-axis basement samples to estimate the Mg isotopic composition of the AOC. Based on the proportions, thicknesses, MgO concentrations and δ^{26}Mg of the four on-axis units, the weighted average δ^{26}Mg of the on-axis basement is estimated to be 0.00 ± 0.09‰. A slightly higher weighted average δ^{26}Mg of 0.02 ± 0.08‰ is obtained by using the MIX composites. These two estimates are identical to the δ^{26}Mg of SUPER composite (−0.02 ± 0.06‰) within analytical uncertainties (±0.07‰). All of these estimated δ^{26}Mg values (−0.02‰ to 0.02‰) are significantly higher than the unaltered oceanic crust (−0.25 ± 0.07‰, Teng et al., 2010a). This robust result requires the preferential retention of heavy Mg isotopes in the bulk AOC during low-temperature alteration of the oceanic crust.

5.4. Implications for the global oceanic Mg cycle

The modern oceans have homogenous Mg concentration (53 mmol/l, Holland et al., 1986) and isotopic composition (−0.83 ± 0.1‰, Ling et al., 2011). However, current global riverine input to the ocean, has a slightly lower δ^{26}Mg (−1.09‰) than modern seawater (Tipper et al., 2006). The Mg isotopic difference between riverine input and seawater suggests that the modern ocean might not be at steady state with respect to Mg isotope ratios, and/or other processes preferentially remove light Mg isotopes from the oceans, such as hydrothermal circulation, marine carbonate deposition (biogenic calcite and dolomite) and low-temperature alteration of the oceanic crust (Fig. 8). Limited Mg isotope fractionation is expected during high-temperature hydrothermal circulation at the ridge axis due to the quantitative removal of Mg (Tipper et al., 2006). As a consequence, carbonate deposition and/or low-temperature alteration of the oceanic crust must be the dominant process for removing light Mg isotopes from the oceans (Ligi et al., 2013; Higgins and Schrag, 2015).

To quantitatively constrain the contribution of low-temperature alteration of the oceanic crust versus carbonate deposition to the Mg cycle in the oceans, we use the following numerical model. The amount of Mg in the oceans (N_{Mg}) changes with time primarily as the result of imbalance between the inputs of Mg from rivers (F_{riv}) and the outputs of Mg through combined high-temperature hydrothermal circulation at the mid-ocean ridges (F_{hyd}), dolomitization (a major Mg sink during carbonate deposition, F_{dol}) and low-temperature alteration of the oceanic crust (F_{AOC}):

$$\frac{dN_{Mg}}{dt} = F_{riv} - F_{hyd} - F_{dol} - F_{AOC} \quad (3)$$

Consequently, the associated change in the Mg isotopic composition of the oceanic Mg reservoir ($\delta^{26}Mg_{sw}$) can be approximately represented as:

$$\begin{aligned}\frac{dN_{Mg}\delta^{26}Mg_{sw}}{dt} = {} & (\delta^{26}Mg_{riv} - \delta^{26}Mg_{sw})F_{riv} \\ & - (\delta^{26}Mg_{hyd} - \delta^{26}Mg_{sw})F_{hyd} \\ & - (\delta^{26}Mg_{dol} - \delta^{26}Mg_{sw})F_{dol} \\ & - (\delta^{26}Mg_{AOC} - \delta^{26}Mg_{sw})F_{AOC} \end{aligned} \quad (4)$$

where $\delta^{26}Mg_{riv}$, $\delta^{26}Mg_{hyd}$,$\delta^{26}Mg_{dol}$, $\delta^{26}Mg_{AOC}$ are Mg isotopic compositions of the riverine input, high-temperature hydrothermal fluid, dolomite formation and altered oceanic crust at low-temperature at time t, respectively. If we assume that the ocean is in a steady state with respect to Mg ($\frac{dN_{Mg}\delta^{26}Mg_{sw}}{dt} = 0$), then the current Mg flux due to low-temperature alteration of the oceanic crust can be estimated by the following isotope mass balance:

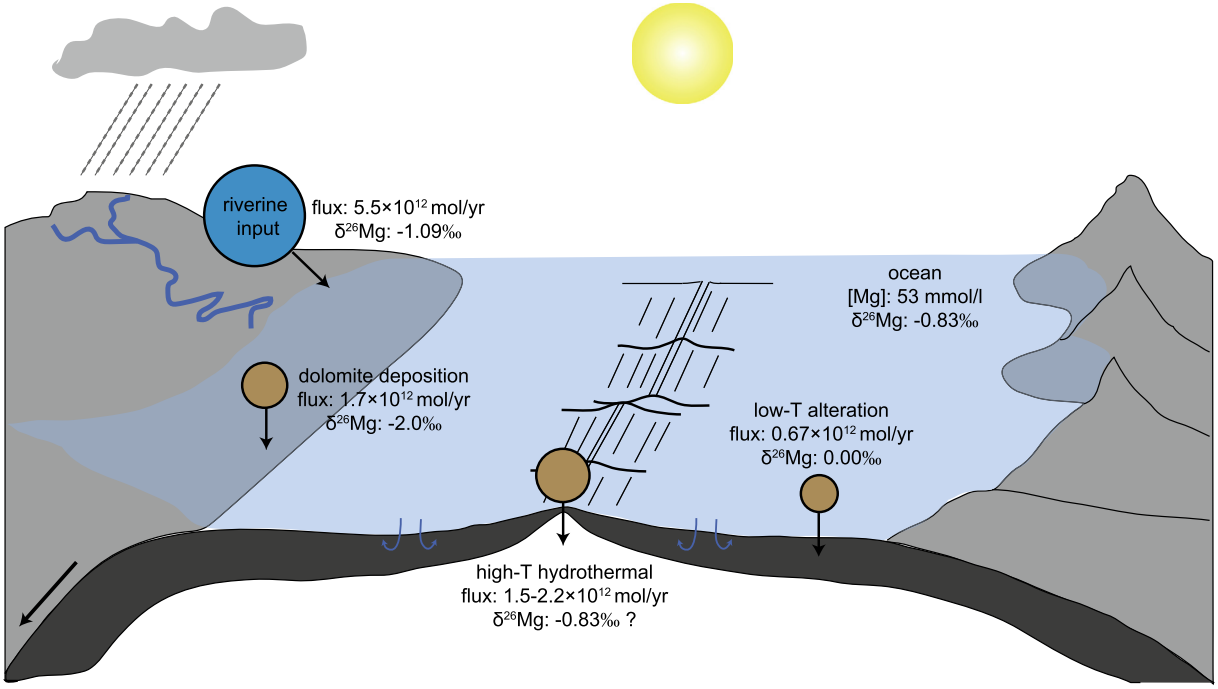

Fig. 8. Cartoon of the global Mg cycle showing the average fluxes and isotopic compositions of the main oceanic sources and sinks of Mg. The directions of the arrows refer to the net uptake or release of Mg for each geological process. The values in the colored boxes refer to δ^{26}Mg values and Mg fluxes of seawater and various inputs/outputs (see text for details). (For interpretation of the references to colour in this figure legend, the reader is referred to the web version of this article.)

$$(\delta^{26}Mg_{riv} - \delta^{26}Mg_{sw})F_{riv} = (\delta^{26}Mg_{hyd} - \delta^{26}Mg_{sw})F_{hyd} + (\delta^{26}Mg_{dol} - \delta^{26}Mg_{sw})F_{dol} + (\delta^{26}Mg_{AOC} - \delta^{26}Mg_{sw})F_{AOC} \quad (5)$$

Given that modern F_{hyd} is $\sim 1.5–2.2 \times 10^{12}$ mol/yr (Elderfield and Schultz, 1996; Nielsen et al., 2006) with a seawater-like δ^{26}Mg, and current F_{dol} is 1.7×10^{12} mol/yr (Holland, 2005) with an average δ^{26}Mg of $-2.0‰$ (Higgins and Schrag, 2010; Fantle and Higgins, 2014), the F_{AOC} is calculated to be $\sim 0.67 \times 10^{12}$ mol/yr if an average $\delta^{26}Mg_{AOC}$ at Site 801 of 0.00‰ is adopted. Although the average δ^{26}Mg of the Mesozoic AOC applied here may be different from the modern one, this calculation offers limits on the direction and magnitude of chemical change for alteration of the oceanic crust at low temperature. This is supported by a similar estimate of $\sim 0.2–0.4 \times 10^{12}$ mol/yr based on chemical analysis of the much younger AOC (~6 Ma) at ODP Holes 504B and 896A (Alt et al., 1996). Our estimated low-temperature Mg sink flux is about 12% of the annual Mg riverine input (Fig. 8), but it is still lower than the missing Mg sink flux (i.e., an additional Mg sink to balance the excess Mg riverine input to the ocean) of at least 1.1×10^{12} mol/yr (Elderfield and Schultz, 1996). Furthermore, in contrast to carbonate deposition, our study shows that the preferential retention of heavy Mg isotopes during low-temperature alteration of the oceanic crust would drive seawater δ^{26}Mg towards lighter values, and thus additional carbonate precipitation is required to maintain seawater in an isotopically steady state. Hence, any attempt to constrain global Mg cycle and Mg isotopic budget through geological history must consider the contribution from this process (Higgins and Schrag, 2015).

5.5. Implications for mantle Mg isotopic heterogeneity

The mantle in general has a homogenous Mg isotopic composition based on a large number of measurements of peridotite xenoliths and oceanic basalts from all over the world (Teng et al., 2007; Handler et al., 2009; Yang et al., 2009; Bourdon et al., 2010; Teng et al., 2010a; Huang et al., 2011; Pogge von Strandmann et al., 2011). However, an increasing number of studies have discovered mantle and mantle-derived rocks with distinct Mg isotope compositions from the prevalent mantle, including metasomatized peridotite xenoliths from the North China Craton (Yang et al., 2009; Xiao et al., 2013; Hu et al., 2016b), continental basalts from East Asia (Yang et al., 2012; Huang et al., 2015b; Tian et al., 2016; Su et al., 2017; Sun et al., 2017) and New Zealand (Wang et al., 2016), and arc lavas from Martinique Island and Philippines (Teng et al., 2016; Li et al., 2017). These isotopically diverse signatures have been attributed to contributions from the down-going oceanic slab and carbonate sediments based on the assumption that the subducted oceanic slab has a Mg isotopic composition different from the mantle (Wang et al., 2012, 2015).

Our results reveal that the AOC has variable δ^{26}Mg, with high values for clay-rich AOC and low values for carbonate-rich AOC (Fig. 9). In addition to AOC, subducting sediments and abyssal peridotites, which are also recycled into the mantle along with the subducting oceanic

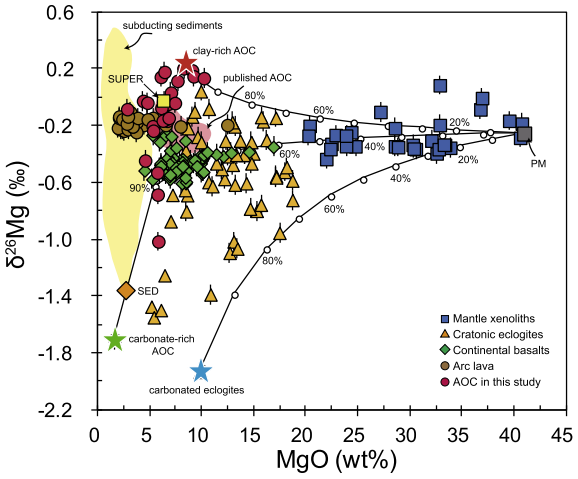

Fig. 9. Plot of MgO contents and δ^{26}Mg values of different geochemical reservoirs. Data sources: cratonic eclogites (Wang et al., 2012; Wang et al., 2014a, 2015; Huang et al., 2016), continental basalts (Yang et al., 2012; Huang et al., 2015b; Tian et al., 2016; Wang et al., 2017), metasomatized peridotites and pyroxenites (Pogge von Strandmann et al., 2011; Xiao et al., 2013; Hu et al., 2016b), subducting sediments (Hu et al., 2017), published AOC (Huang et al., 2015a; Zhong et al., 2017). "PM", "SED" and "SUPER" represent the primary mantle (Teng et al., 2010a), sediment composite and SUPER composite, respectively (this study). Red, green, and blue stars represent clay-rich AOC, carbonate-rich AOC and carbonated eclogite end-members, respectively. The dotted solid lines represent binary mixing between clay-rich AOC and the primary mantle, and between carbonate-rich AOC and the primary mantle, respectively. The numbers along the mixing lines refer to the fractional contributions from these end-members. (For interpretation of the references to colour in this figure legend, the reader is referred to the web version of this article.)

slab (Plank, 2005; Chauvel et al., 2008), have heterogeneous Mg isotopic compositions (Teng et al., 2016; Hu et al., 2017; Liu et al., 2017) (Fig. 9). These isotopically heterogeneous materials can be delivered to the mantle by subduction, potentially with limited isotope fractionation during metamorphic dehydration (Li et al., 2011, 2014; Teng et al., 2013; Wang et al., 2014b). Given the large Mg isotopic variation of the AOC, which is well beyond the Mg isotopic range of mantle xenoliths and mantle-derived volcanic rocks (Fig. 9), it is reasonable to speculate that recycling of the subducted materials into the mantle could produce Mg isotopic diversity in the mantle (Yang et al., 2012; Xiao et al., 2013; Huang et al., 2015b; Hu et al., 2016b; Teng et al., 2016; Tian et al., 2016).

Simple binary mixing between ambient mantle and AOC cannot account for the heterogeneous mantle-derived volcanic rocks because an unrealistic amount of recycled AOC (>70%) is required (Fig. 9). However, partial melting of isotopically heterogeneous AOC, as analyzed in this study and in previous studies on cratonic eclogites (Wang et al., 2012; 2015), can produce isotopically anomalous melts. If these melts react with subcontinental lithospheric mantle, isotopically heterogeneous metasomatized mantle rocks such as wehrlites and pyroxenites can be produced (Xiao et al., 2013; Hu et al., 2016b). Alternatively, if these melts mix with melts derived from the normal mantle, they may form continental basalts with atypical Mg isotopic composition, such as the HIMU-like basalts from New Zealand (Wang et al., 2016). Therefore, subduction of highly heterogeneous AOC along with sediments has the potential to produce Mg isotopic heterogeneity in the mantle on a local scale.

6. CONCLUSIONS

To investigate the behavior of Mg isotopes during low-temperature alteration of the oceanic crust and the influence of this process on the global Mg cycle, we present high-precision Mg isotopic data of the individual and composite AOC samples recovered from the ODP Hole 801C, the reference site for old crust subducted in the Pacific. The following conclusions can be drawn:

(1) Compared to fresh MORB, δ^{26}Mg values of individual and composite AOC samples are highly heterogeneous, varying from −1.70‰ to 0.21‰, which requires large Mg isotope fractionation during low-temperature alteration of the oceanic crust.
(2) Saponite, which forms under anoxic conditions with low water/rock ratios and high pH in the deeper on-axis basement, preferentially incorporates heavy Mg isotopes and leads to the high δ^{26}Mg values. By contrast, calcite, which precipitates under open and more oxidative upper off-axis basement, preferentially takes up light Mg isotopes. These carbonates, together with accumulation of interflow sediments, result in the low δ^{26}Mg values in the off-axis basement.
(3) A weighted average δ^{26}Mg value of the AOC at Site 801 is estimated to be 0.00 ± 0.09‰. The Mg sink flux due to low-temperature alteration of the oceanic crust is estimated as $\sim 0.67 \times 10^{12}$ mol/yr (i.e., 12% of the current yearly Mg riverine input) based on a first-order mass balance calculation, suggesting that alteration of the oceanic crust at low temperature serves as an important sink to balance seawater Mg budget.
(4) Subduction of AOC, along with its marine sedimentary cover, introduces material with highly variable Mg isotopic compositions into the mantle, and thus is likely to generate mantle Mg isotopic heterogeneity on a local scale.

ACKNOWLEDGMENTS

We acknowledge the Ocean Drilling Program for providing the samples for this study, Dabra A. Wallance, Fatemeh Sedaghatpour and Shui-Jiong Wang for help in the lab, and Bing Shen for stimulating discussions. John Higgins, two anonymous reviewers and the associate editor Jeff Alt are thanked for their insightful comments that greatly improved the manuscript. This work is financially supported by the Natural Science Foundation of China (41602343; 41621003; 41729001; 41427804), the U.S. National Science Foundation (EAR-1747706), and the "111" project (D17013).

APPENDIX A. SUPPLEMENTARY MATERIAL

Supplementary data associated with this article can be found, in the online version, at https://doi.org/10.1016/j.gca.2018.07.011.

REFERENCES

Alt J. C. (2003a) Hydrothermal fluxes at mid-ocean ridges and on ridge flanks. *C.R. Geosci.* **335**, 853–864.

Alt J. C. (2003b) Stable isotopic composition of upper oceanic crust formed at a fast spreading ridge, ODP Site 801. *Geochem. Geophys. Geosyst.* **4**, 8908.

Alt J. C. (2004) Alteration of the upper oceanic crust: mineralogy, chemistry, and processes. In *Hydrogeology of the Oceanic Lithosphere* (eds. E. E. Davis and H. Elderfield). Cambridge University Press, New York, pp. 495–533.

Alt J. C., France-Lanord C., Floyd P. A., Castillo P., Gal A. (1992) Low Temperature Hydrothermal Alteration of Jurassic Ocean Crust, Site 801. Ocean Drilling Program, College Station, TX.

Alt J. C. and Teagle D. A. H. (1999) The uptake of carbon during alteration of ocean crust. *Geochim. Cosmochim. Acta* **63**, 1527–1535.

Alt J. C. and Teagle D. A. H. (2003) Hydrothermal alteration of upper oceanic crust formed at a fast-spreading ridge: mineral, chemical, and isotopic evidence from ODP Site 801. *Chem. Geol.* **201**, 191–211.

Alt J. C., Teagle D. A. H., Laverne C., Vanko D. A., Bach W., Honnorez J., Becker K., Ayadi M. and Pezard P. A. (1996) Ridge-flank alteration of upper ocean crust in the eastern Pacific: synthesis of results for volcanic rocks of Holes 504B and 896A. In *Proceedings of the ocean drilling program, Scientific results* (eds. J. C. Alt, H. Kinoshita, L. B. Stokking and P. J. Michael). Ocean Drilling Program, College Station, TX, pp. 435–450.

Bartolini A. and Larson R. L. (2001) Pacific microplate and the Pangea supercontinent in the Early to Middle Jurassic. *Geology* **29**, 735–738.

Bourdon B., Tipper E. T., Fitoussi C. and Stracke A. (2010) Chondritic Mg isotope composition of the Earth. *Geochim. Cosmochim. Acta* **74**, 5069–5083.

Chan L.-H., Alt J. C. and Teagle D. A. H. (2002) Lithium and lithium isotope profiles through the upper oceanic crust: a study of seawater–basalt exchange at ODP Sites 504B and 896A. *Earth Planet. Sci. Lett.* **201**, 187–201.

Chauvel C., Lewin E., Carpentier M., Arndt N. T. and Marini J.-C. (2008) Role of recycled oceanic basalt and sediment in generating the Hf-Nd mantle array. *Nat. Geosci.* **1**, 64–67.

Coggon R. M. and Teagle D. A. H. (2011) Hydrothermal calcium-carbonate veins reveal past ocean chemistry. *Trends Anal. Chem.* **30**, 1252–1268.

Coogan L. A. and Gillis K. M. (2013) Evidence that low-temperature oceanic hydrothermal systems play an important role in the silicate-carbonate weathering cycle and long-term climate regulation. *Geochem. Geophys. Geosyst.* **14**, 1771–1786.

Cooper K. M., Eiler J. M., Sims K. W. W. and Langmuir C. H. (2009) Distribution of recycled crust within the upper mantle: insights from the oxygen isotope composition of MORB from the Australian-Antarctic Discordance. *Geochem. Geophys. Geosyst.* **10**, Q12004.

Demicco R. V., Lowenstein T. K., Hardie L. A. and Spencer R. J. (2005) Model of seawater composition for the Phanerozoic. *Geology* **33**, 877–880.

Drever J. I. (1974) The magnesium problem. In *Marine Chemistry. The Sea: Ideas and Observations on Progress in the Study of the Seas* (ed. E. D. Goldberg). Wiley Interscience, New York, pp. 337–357.

Elderfield H. and Schultz A. (1996) Mid-ocean ridge hydrothermal fluxes and the chemical composition of the ocean. *Annu. Rev. Earth Planet. Sci.* **24**, 191–224.

Elderfield H., Wheat C. G., Mottl M. J., Monnin C. and Spiro B. (1999) Fluid and geochemical transport through oceanic crust: a transect across the eastern flank of the Juan de Fuca Ridge. *Earth Planet. Sci. Lett.* **172**, 151–165.

Fantle M. S. and Higgins J. (2014) The effects of diagenesis and dolomitization on Ca and Mg isotopes in marine platform carbonates: implications for the geochemical cycles of Ca and Mg. *Geochim. Cosmochim. Acta* **142**, 458–481.

Fisher A. T. (1998) Permeability within basaltic oceanic crust. *Rev. Geophys.* **36**, 143–182.

Fisk M. and Kelley K. A. (2002) Probing the Pacific's oldest MORB glass: mantle chemistry and melting conditions during the birth of the Pacific Plate. *Earth Planet. Sci. Lett.* **202**, 741–752.

Foster G. L., Pogge von Strandmann P. A. E. and Rae J. W. B. (2010) Boron and magnesium isotopic composition of seawater. *Geochem. Geophys. Geosyst.* **11**, Q08015.

Gale A., Dalton C. A., Langmuir C. H., Su Y. and Schilling J. G. (2013) The mean composition of ocean ridge basalts. *Geochem. Geophys. Geosyst.* **14**, 489–518.

Gillis K. M. and Coogan L. A. (2011) Secular variation in carbon uptake into the ocean crust. *Earth Planet. Sci. Lett.* **302**, 385–392.

Handler M. R., Baker J. A., Schiller M., Bennett V. C. and Yaxley G. M. (2009) Magnesium stable isotope composition of Earth's upper mantle. *Earth Planet. Sci. Lett.* **282**, 306–313.

Hardie L. A. (1996) Secular variation in seawater chemistry: an explanation for the coupled secular variation in the mineralogies of marine limestones and potash evaporites over the past 600 m.y. *Geology* **24**, 279–283.

Hart S. R., Erlank A. J. and Kable E. J. D. (1974) Sea floor basalt alteration: some chemical and Sr isotopic effects. *Contrib. Mineral. Petrol.* **44**, 219–230.

Higgins J. A. and Schrag D. P. (2010) Constraining magnesium cycling in marine sediments using magnesium isotopes. *Geochim. Cosmochim. Acta* **74**, 5039–5053.

Higgins J. A. and Schrag D. P. (2015) The Mg isotopic composition of Cenozoic seawater – evidence for a link between Mg-clays, seawater Mg/Ca, and climate. *Earth Planet. Sci. Lett.* **416**, 73–81.

Hofmann A. W. (1997) Mantle geochemistry: the message from oceanic volcanism. *Nature* **385**, 219–229.

Holland H. D. (2005) Sea level, sediments and the composition of seawater. *Am. J. Sci.* **305**, 220–239.

Holland H. D., Lazar B. and McCaffrey M. (1986) Evolution of the atmosphere and oceans. *Nature* **320**, 27–33.

Hu Y., Harrington M. D., Sun Y., Yang Z., Konter J. and Teng F.-Z. (2016a) Magnesium isotopic homogeneity of San Carlos olivine: a potential standard for Mg isotopic analysis by multi-collector inductively coupled plasma mass spectrometry. *Rapid Commun. Mass Spectrom.* **30**, 2123–2132.

Hu Y., Teng F.-Z., Plank T. and Huang K.-J. (2017) Magnesium isotopic composition of subducting marine sediments. *Chem. Geol.* **466**, 15–31.

Hu Y., Teng F.-Z., Zhang H.-F., Xiao Y. and Su B.-X. (2016b) Metasomatism-induced mantle magnesium isotopic heterogeneity: evidence from pyroxenites. *Geochim. Cosmochim. Acta* **185**, 88–111.

Huang F., Zhang Z., Lundstrom C. C. and Zhi X. (2011) Iron and magnesium isotopic compositions of peridotite xenoliths from Eastern China. *Geochim. Cosmochim. Acta* **75**, 3318–3334.

Huang J.-X., Xiang Y., An Y., Griffin W. L., Gréau Y., Xie L., Pearson N. J., Yu H. and O'Reilly S. Y. (2016) Magnesium and oxygen isotopes in Roberts Victor eclogites. *Chem. Geol.* **438**, 73–83.

Huang J., Ke S., Gao Y., Xiao Y. and Li S. (2015a) Magnesium isotopic compositions of altered oceanic basalts and gabbros from IODP Site 1256 at the East Pacific Rise. *Lithos* **231**, 53–61.

Huang J., Li S.-G., Xiao Y., Ke S., Li W.-Y. and Tian Y. (2015b) Origin of low δ^{26}Mg Cenozoic basalts from South China Block and their geodynamic implications. *Geochim. Cosmochim. Acta* **164**, 298–317.

Huang K.-J., Shen B., Lang X.-G., Tang W.-B., Peng Y., Ke S., Kaufman A. J., Ma H.-R. and Li F.-B. (2015c) Magnesium isotopic compositions of the Mesoproterozoic dolostones: implications for Mg isotopic systematics of marine carbonates. *Geochim. Cosmochim. Acta* **164**, 333–351.

Humphris S. E. and Thompson G. (1978) Trace element mobility during hydrothermal alteration of oceanic basalts. *Geochim. Cosmochim. Acta* **42**, 127–136.

Kastner M. and Gieskes J. M. (1976) Interstitial water profiles and sites of diagenetic reactions, Leg 35, DSDP, Bellingshausen Abyssal Plain. *Earth Planet. Sci. Lett.* **33**, 11–20.

Kelley K. A., Plank T., Farr L., Ludden J. and Staudigel H. (2005) Subduction cycling of U, Th, and Pb. *Earth Planet. Sci. Lett.* **234**, 369–383.

Kelley K. A., Plank T., Ludden J. and Staudigel H. (2003) Composition of altered oceanic crust at ODP Sites 801 and 1149. *Geochem. Geophys. Geosyst.* **4**, 8910.

Klein E. M. (2003) 3.13 - Geochemistry of the igneous oceanic crust Editors-in-Chief:. In *Treatise on Geochemistry* (eds. D. H. Heinrich and K. T. Karl). Pergamon, Oxford, pp. 433–463.

Koppers A. A. P., Staudigel H. and Duncan R. A. (2003) High-resolution ^{40}Ar/^{39}Ar dating of the oldest oceanic basement basalts in the western Pacific basin. *Geochem. Geophys. Geosyst.* **4**, 8914.

Li S.-G., Yang W., Ke S., Meng X., Tian H., Xu L., He Y., Huang J., Wang X.-C., Xia Q., Sun W., Yang X., Ren Z.-Y., Wei H., Liu Y., Meng F. and Yan J. (2017) Deep carbon cycles constrained by a large-scale mantle Mg isotope anomaly in eastern China. *Natl. Sci. Rev.* **4**, 111–120.

Li W.-Y., Teng F.-Z., Ke S., Rudnick R. L., Gao S., Wu F.-Y. and Chappell B. W. (2010) Heterogeneous magnesium isotopic composition of the upper continental crust. *Geochim. Cosmochim. Acta* **74**, 6867–6884.

Li W.-Y., Teng F.-Z., Wing B. A. and Xiao Y. (2014) Limited magnesium isotope fractionation during metamorphic dehydration in metapelites from the Onawa contact aureole. *Maine. Geochem. Geophys. Geosyst.* **15**, 408–415.

Li W.-Y., Teng F.-Z., Xiao Y. and Huang J. (2011) High-temperature inter-mineral magnesium isotope fractionation in eclogite from the Dabie orogen, China. *Earth Planet. Sci. Lett.* **304**, 224–230.

Ligi M., Bonatti E., Cuffaro M. and Brunelli D. (2013) Post-mesozoic rapid increase of seawater Mg/Ca due to enhanced mantle-seawater interaction. *Sci. Rep.* **3**, 1–8.

Ling M.-X., Liu Y.-L., Williams I. S., Teng F.-Z., Yang X.-Y., Ding X., Wei G.-J., Xie L.-H., Deng W.-F. and Sun W.-D. (2013) Formation of the world's largest REE deposit through protracted fluxing of carbonatite by subduction-derived fluids. *Sci. Rep.* **3**, 1–8.

Ling M.-X., Sedaghatpour F., Teng F.-Z., Hays P. D., Strauss J. and Sun W. (2011) Homogeneous magnesium isotopic composition of seawater: an excellent geostandard for Mg isotope analysis. *Rapid Commun. Mass Spectrom.* **25**, 2828–2836.

Liu D., Zhao Z., Zhu D.-C., Niu Y., Widom E., Teng F.-Z., DePaolo D. J., Ke S., Xu J.-F., Wang Q. and Mo X. (2015) Identifying mantle carbonatite metasomatism through Os–Sr–Mg isotopes in Tibetan ultrapotassic rocks. *Earth Planet. Sci. Lett.* **430**, 458–469.

Liu P.-P., Teng F.-Z., Dick H. J. B., Zhou M.-F. and Chung S.-L. (2017) Magnesium isotopic composition of the oceanic mantle and oceanic Mg cycling. *Geochim. Cosmochim. Acta* **206**, 151–165.

Ludden J. N., Plank T., Larson R. and Escutia C. (2006) Leg 185 synthesis: sampling the oldest crust in the ocean basins to understand earth's geodynamic and geochemical fluxes. In *Proceedings of the Ocean Drilling Program* (eds. J. N. Ludden, T. Plank and C. Escutia). Scientific Results, pp. 1–35.

MacLean W. H. and Barrett T. J. (1993) Lithogeochemical techniques using immobile elements. *J. Geochem. Explor.* **48**, 109–133.

Mottl M. J. (2003) Partitioning of energy and mass fluxes between mid-ocean ridge axes and flanks at high and low temperature. In *Energy and Mass Transfer in Marine Hydrothermal Systems* (eds. P. Halbach, V. Tunnicliffe and J. R. Hein). Dahlem University Press, Berlin, pp. 271–286.

Mottl M. J. and Wheat C. G. (1994) Hydrothermal circulation through mid-ocean ridge flanks: fluxes of heat and magnesium. *Geochim. Cosmochim. Acta* **58**, 2225–2237.

Muehlenbachs K. and Clayton R. N. (1972) Oxygen isotope studies of fresh and weathered submarine basalts. *Can. J. Earth Sci.* **9**, 172–184.

Nielsen S. G., Rehkämper M., Teagle D. A. H., Butterfield D. A., Alt J. C. and Halliday A. N. (2006) Hydrothermal fluid fluxes calculated from the isotopic mass balance of thallium in the ocean crust. *Earth Planet. Sci. Lett.* **251**, 120–133.

Oeser M., Weyer S., Horn I. and Schuth S. (2014) High-precision Fe and Mg isotope ratios of silicate reference glasses determined in situ by femtosecond LA-MC-ICP-MS and by solution nebulisation MC-ICP-MS. *Geostand. Geoanal. Res.* **38**, 311–328.

Plank T. (2005) Constraints from thorium/lanthanum on sediment recycling at subduction zones and the evolution of the continents. *J. Petrol.* **46**, 921–944.

Plank T., Ludden J. N., Escutia C. (2000) Site 801. In Proceedings of the Ocean Drilling Program, Initial Reports, College Station, TX (eds. T. Plank, J. N. Ludden and C. Escutia). pp. 1–222.

Pogge von Strandmann P. A. E., Elliott T., Marschall H. R., Coath C., Lai Y.-J., Jeffcoate A. B. and Ionov D. A. (2011) Variations of Li and Mg isotope ratios in bulk chondrites and mantle xenoliths. *Geochim. Cosmochim. Acta* **75**, 5247–5268.

Ryu J.-S., Jacobson A. D., Holmden C., Lundstrom C. and Zhang Z. (2011) The major ion, $\delta^{44/40}$Ca, $\delta^{44/42}$Ca, and $\delta^{26/24}$Mg geochemistry of granite weathering at pH = 1 and T = 25°C: power-law processes and the relative reactivity of minerals. *Geochim. Cosmochim. Acta* **75**, 6004–6026.

Ryu J.-S., Vigier N., Decarreau A., Lee S.-W., Lee K.-S., Song H. and Petit S. (2016) Experimental investigation of Mg isotope fractionation during mineral dissolution and clay formation. *Chem. Geol.* **445**, 135–145.

Saenger C. and Wang Z. (2014) Magnesium isotope fractionation in biogenic and abiogenic carbonates: implications for paleoenvironmental proxies. *Quat. Sci. Rev.* **90**, 1–21.

Saulnier S., Rollion-Bard C., Vigier N. and Chaussidon M. (2012) Mg isotope fractionation during calcite precipitation: an experimental study. *Geochim. Cosmochim. Acta* **91**, 75–91.

Seyfried W. E. Jr. and Bischoff J. L. (1979) Low temperature basalt alteration by sea water: an experimental study at 70°C and 150° C. *Geochim. Cosmochim. Acta* **43**, 1937–1947.

Seyfried W. E. Jr., Janecky D. R. and Mottl M. J. (1984) Alteration of the oceanic crust: Implications for geochemical cycles of lithium and boron. *Geochim. Cosmochim. Acta* **48**, 557–569.

Seyfried W. E. Jr., Shanks Iii W. C. and Dibble, Jr, W. E. (1978) Clay mineral formation in DSDP Leg 34 basalt. *Earth Planet. Sci. Lett.* **41**, 265–276.

Smith H. J., Spivack A. J., Staudigel H. and Hart S. R. (1995) The boron isotopic composition of altered oceanic crust. *Chem. Geol.* **126**, 119–135.

Stanley S. M. and Hardie L. A. (1998) Secular oscillations in the carbonate mineralogy of reef-building and sediment-producing organisms driven by tectonically forced shifts in seawater chemistry. *Palaeogeogr. Palaeoclimatol. Palaeoecol.* **144**, 3–19.

Staudigel H. (2003) Hydrothermal alteration processes in the oceanic crust. In *Treatise on Geochemistry*. (eds. D. H. Heinrich and K. T. Karl). Pergamon, Oxford, pp. 511–535.

Staudigel H. (2014) Chemical fluxes from hydrothermal alteration of the oceanic crust. In *Treatise on Geochemistry* (ed. H. D. H. K. Turekian), second ed. Elsevier, Oxford, pp. 583–606.

Staudigel H., Davies G. R., Hart S. R., Marchant K. M. and Smith B. M. (1995) Large scale isotopic Sr, Nd and O isotopic anatomy of altered oceanic crust: DSDP/ODP sites417/418. *Earth Planet. Sci. Lett.* **130**, 169–185.

Staudigel H., Hart S. R., Schmincke H.-U. and Smith B. M. (1989) Cretaceous ocean crust at DSDP Sites 417 and 418: carbon uptake from weathering versus loss by magmatic outgassing. *Geochim. Cosmochim. Acta* **53**, 3091–3094.

Staudigel H., Plank T., White B. and Schmincke H.-U. (1996) Geochemical fluxes during seafloor alteration of the basaltic upper oceanic crust: DSDP sites 417 and 418. In *Subduction: Top to Bottom* (eds. E. Bebout, W. Scholl, H. Kirby and P. Platt). AGU, Washington, D.C., pp. 19–38.

Su B.-X., Hu Y., Teng F.-Z., Xiao Y., Zhou X.-H., Sun Y., Zhou M.-F. and Chang S.-C. (2017) Magnesium isotope constraints on subduction contribution to Mesozoic and Cenozoic East Asian continental basalts. *Chem. Geol.* **466**, 116–122.

Sun Y., Teng F.-Z., Ying J.-F., Su B.-X., Hu Y., Fan Q.-C. and Zhou X.-H. (2017) Magnesium isotopic evidence for ancient subducted oceanic crust in LOMU-like potassium-rich volcanic rocks. *J. Geophys. Res.: Solid Earth* **122**, 7562–7572.

Talbi E. H. and Honnorez J. (2003) Low-temperature alteration of mesozoic oceanic crust, Ocean Drilling Program Leg 185. *Geochem. Geophys. Geosyst.* **4**, 8906.

Teng F.-Z., Hu Y. and Chauvel C. (2016) Magnesium isotope geochemistry in arc volcanism. *Proc. Natl. Acad. Sci. USA* **113**, 7082–7087.

Teng F.-Z., Li W.-Y., Ke S., Marty B., Dauphas N., Huang S., Wu F.-Y. and Pourmand A. (2010a) Magnesium isotopic composition of the Earth and chondrites. *Geochim. Cosmochim. Acta* **74**, 4150–4166.

Teng F.-Z., Li W.-Y., Ke S., Yang W., Liu S.-A., Sedaghatpour F., Wang S.-J., Huang K.-J., Hu Y., Ling M.-X., Xiao Y., Liu X.-M., Li X.-W., Gu H.-O., Sio C. K., Wallace D. A., Su B.-X., Zhao L., Chamberlin J., Harrington M. and Brewer A. (2015) Magnesium isotopic compositions of international geostandards. *Geostand. Geoanal. Res.* **39**, 329–339.

Teng F.-Z., Li W.-Y., Rudnick R. L. and Gardner L. R. (2010b) Contrasting lithium and magnesium isotope fractionation during continental weathering. *Earth Planet. Sci. Lett.* **300**, 63–71.

Teng F.-Z., Wadhwa M. and Helz R. T. (2007) Investigation of magnesium isotope fractionation during basalt differentiation: implications for a chondritic composition of the terrestrial mantle. *Earth Planet. Sci. Lett.* **261**, 84–92.

Teng F.-Z. and Yang W. (2014) Comparison of factors affecting accuracy of high-precision magnesium isotope analysis by MC-ICPMS. *Rapid Commun. Mass Spectrom.* **28**, 19–24.

Teng F.-Z., Yang W., Rudnick R. L. and Hu Y. (2013) Heterogeneous magnesium isotopic composition of the lower continental crust: a xenolith perspective. *Geochem. Geophys. Geosyst.* **14**, 3844–3856.

Tian H.-C., Yang W., Li S.-G., Ke S. and Chu Z.-Y. (2016) Origin of low δ^{26}Mg basalts with EM-I component: evidence for interaction between enriched lithosphere and carbonated asthenosphere. *Geochim. Cosmochim. Acta* **188**, 93–105.

Tipper E. T., Galy A., Gaillardet J., Bickle M. J., Elderfield H. and Carder E. A. (2006) The magnesium isotope budget of the modern ocean: constraints from riverine magnesium isotope ratios. *Earth Planet. Sci. Lett.* **250**, 241–253.

Wang S.-J., Teng F.-Z. and Li S.-G. (2014a) Tracing carbonate–silicate interaction during subduction using magnesium and oxygen isotopes. *Nat. Commun.* **5**. https://doi.org/10.1038/ncomms6328.

Wang S.-J., Teng F.-Z., Li S.-G. and Hong J.-A. (2014b) Magnesium isotopic systematics of mafic rocks during continental subduction. *Geochim. Cosmochim. Acta* **143**, 34–48.

Wang S.-J., Teng F.-Z., Rudnick R. L. and Li S.-G. (2015) Magnesium isotope evidence for a recycled origin of cratonic eclogites. *Geology* **43**, 1071–1074.

Wang S.-J., Teng F.-Z. and Scott J. M. (2016) Tracing the origin of continental HIMU-like intraplate volcanism using magnesium isotope systematics. *Geochim. Cosmochim. Acta* **185**, 78–87.

Wang S.-J., Teng F.-Z., Williams H. M. and Li S.-G. (2012) Magnesium isotopic variations in cratonic eclogites: origins and implications. *Earth Planet. Sci. Lett.* **359–360**, 219–226.

Wang X.-J., Chen L.-H., Hofmann A. W., Mao F.-G., Liu J.-Q., Zhong Y., Xie L.-W. and Yang Y.-H. (2017) Mantle transition zone-derived EM1 component beneath NE China: geochemical evidence from Cenozoic potassic basalts. *Earth Planet. Sci. Lett.* **465**, 16–28.

Wheat C. G. and Fisher A. T. (2008) Massive, low-temperature hydrothermal flow from a basaltic outcrop on 23 Ma seafloor of the Cocos Plate: Chemical constraints and implications. *Geochem. Geophys. Geosyst.* **9**, Q12O14.

Wiechert U. and Halliday A. N. (2007) Non-chondritic magnesium and the origins of the inner terrestrial planets. *Earth Planet. Sci. Lett.* **256**, 360–371.

Wimpenny J., Gíslason S. R., James R. H., Gannoun A., Pogge Von Strandmann P. A. E. and Burton K. W. (2010) The behaviour of Li and Mg isotopes during primary phase dissolution and secondary mineral formation in basalt. *Geochim. Cosmochim. Acta* **74**, 5259–5279.

Wimpenny J., Yin Q.-Z., Tollstrup D., Xie L.-W. and Sun J. (2014) Using Mg isotope ratios to trace Cenozoic weathering changes: A case study from the Chinese loess plateau. *Chem. Geol.* **376**, 31–43.

Wombacher F., Eisenhauer A., Heuser A. and Weyer S. (2009) Separation of Mg, Ca and Fe from geological reference materials for stable isotope ratio analyses by MC-ICP-MS and double-spike TIMS. *J. Anal. At. Spectrom.* **24**, 627–636.

Xiao Y., Teng F.-Z., Zhang H.-F. and Yang W. (2013) Large magnesium isotope fractionation in peridotite xenoliths from eastern North China craton: product of melt-rock interaction. *Geochim. Cosmochim. Acta* **115**, 241–261.

Yang W., Teng F.-Z. and Zhang H.-F. (2009) Chondritic magnesium isotopic composition of the terrestrial mantle: a case study of peridotite xenoliths from the North China craton. *Earth Planet Sci. Lett.* **288**, 475–482.

Yang W., Teng F.-Z., Zhang H.-F. and Li S.-G. (2012) Magnesium isotopic systematics of continental basalts from the North China craton: implications for tracing subducted carbonate in the mantle. *Chem. Geol.* **328**, 185–194.

Zhong Y., Chen L.-H., Wang X.-J., Zhang G.-L., Xie L.-W. and Zeng G. (2017) Magnesium isotopic variation of oceanic island basalts generated by partial melting and crustal recycling. *Earth Planet. Sci. Lett.* **463**, 127–135.

Associate editor: Jeffrey C. Alt